

The Antioxidative Role of Cytoglobin in Podocytes: Implications for a Role in Chronic Kidney Disease

Elisa B. Randi,¹⁻³ Benjamin Vervaet,⁴ Maria Tsachaki,^{3,5} Elena Porto,⁶ Stijn Vermeulen,⁴ Maja T. Lindenmeyer,^{2,3,7} Le Thi Thanh Thuy,⁸ Clemens D. Cohen,^{2,3,7} Olivier Devuyst,^{2,3} Andreas D. Kistler,⁹ Csaba Szabo,¹⁰ Norifumi Kawada,⁸ Thomas Hankeln,⁶ Alex Odermatt,^{3,5} Sylvia Dewilde,⁴ Roland H. Wenger,^{2,3} and David Hoogewijs^{1,3}

Abstract

Aims: Cytoglobin (CYGB) is a member of the mammalian globin family of respiratory proteins. Despite extensive research efforts, its physiological role remains largely unknown, but potential functions include reactive oxygen species (ROS) detoxification and signaling. Accumulating evidence suggests that ROS play a crucial role in podocyte detachment and apoptosis during diabetic kidney disease. This study aimed to explore the potential antioxidative renal role of CYGB both *in vivo* and *in vitro*.

Results: Using a *Cygb*-deficient mouse model, we demonstrate a *Cygb*-dependent reduction in renal function, coinciding with a reduced number of podocytes. To specifically assess the putative antioxidative function of CYGB in podocytes, we first confirmed high endogenous CYGB expression levels in two human podocyte cell lines and subsequently generated short hairpin RNA-mediated stable CYGB knockdown podocyte models. CYGB-deficient podocytes displayed increased cell death and accumulation of ROS as assessed by 2',7'-dichlorodihydrofluorescein diacetate assays and the redox-sensitive probe roGFP2-Orp1. CYGB-deficient cells also exhibited an impaired cellular bioenergetic status. Consistently, analysis of the CYGB-dependent transcriptome identified dysregulation of multiple genes involved in redox balance, apoptosis, as well as in chronic kidney disease (CKD). Finally, genome-wide association studies and expression studies in nephropathy biopsies indicate an association of CYGB with CKD.

Innovation: This study demonstrates a podocyte-related renal role of *Cygb*, confirms abundant CYGB expression in human podocyte cell lines, and describes for the first time an association between CYGB and CKD.

Conclusion: Our results provide evidence for an antioxidative role of CYGB in podocytes. *Antioxid. Redox Signal.* 32, 1155–1171.

Keywords: oxidative stress, reactive oxygen species, globin, diabetic nephropathy

¹Department of Medicine/Physiology, University of Fribourg, Fribourg, Switzerland.

²Institute of Physiology and Zurich Center for Integrative Human Physiology (ZIHP), University of Zurich, Zurich, Switzerland.

³National Centre of Competence in Research (NCCR) "Kidney.CH", Zurich, Switzerland.

⁴Department of Biomedical Sciences, University of Antwerp, Antwerp, Belgium.

⁵Division of Molecular and Systems Toxicology, Department of Pharmaceutical Sciences, University of Basel, Basel, Switzerland.

⁶Institute of Organismal and Molecular Evolutionary Biology, University of Mainz, Mainz, Germany.

⁷Nephrological Center, Medical Clinic and Policlinic IV, University of Munich, Munich, Germany.

⁸Department of Hepatology, Graduate School of Medicine, Osaka City University, Osaka, Japan.

⁹Division of Nephrology, Kantonsspital Frauenfeld, Frauenfeld, Switzerland.

¹⁰Chair of Pharmacology, Faculty of Science and Medicine, University of Fribourg, Fribourg, Switzerland.

Innovation

Cytoglobin (Cygb) represents the fourth recently identified globin in humans. The renal role of Cygb has not been extensively explored. Our findings indicate a previously undiscovered podocyte-related renal role of Cygb, confirm abundant Cygb expression in human podocyte cell lines, provide evidence for an antioxidative role of Cygb in podocytes, and describe for the first time an association between Cygb and chronic kidney disease.

Introduction

CYTOGLOBIN (Cygb) belongs to the family of mammalian globins in addition to hemoglobin (Hb), myoglobin (Mb), neuroglobin (Ngb), and the recently identified androglobin (Adgb) (6). Most known globins fulfill respiratory functions, supplying the cell with adequate amounts of O₂ for aerobic energy production *via* the respiratory chain in the mitochondria (72). In contrast to Mb and Hb, the more recently identified globins Cygb (5, 7), Ngb (5, 7), as well as Adgb (27) all display hexacoordination of the heme iron atom (*i.e.*, bound by two amino acid residues of the globin fold). While no functional interpretation for this heme hexacoordination currently exists, it is thought to point at a role other than the classical oxygen delivery and supply of Hb and Mb. The tissue expression profile of mammalian Cygb has been extensively studied (25). Cygb is predominantly expressed in fibroblasts and related cell types, and also in distinct nerve cell populations. Its physiological function, however, remains unclear; potentially, Cygb may have a role in oxygen storage, NO metabolism, and ROS protection or signaling.

Several animal model studies assessed the functional role of Cygb. Singh *et al.* (60) suggested a major role of Cygb in muscle repair and regeneration as myogenic progenitor cells derived from a mouse model, in which Cygb was specifically knocked out in skeletal muscle, were severely deficient in their ability to form myotubes. Moreover, Thuy *et al.* (66) support the antioxidant role of Cygb using a global knockout mouse model, which displays age-dependent development of multiple organ abnormalities. Using the same Cygb-deficient model, Liu *et al.* (36) recently provided evidence for a role of Cygb as regulator of NO degradation and cardiovascular tone in the vascular wall, in line with their previous *in vitro* observations on the NO dioxygenase function of Cygb (37). In addition, Thuy *et al.* (64) and Yassin *et al.* (75) both reported an implication of Cygb in tumorigenesis using *in vivo* models.

The renal role of Cygb has been underexplored. Nakatani *et al.* (48) detected expression of Cygb in rat kidney, mainly in fibroblasts, and also in the glomerulus. Upon cyclosporine A-induced nephropathy, *Cygb* expression was upregulated in fibrotic lesions of the kidney, specifically in interstitial fibroblasts positive for renal fibroblast markers CD73 and α SMA. Thuy *et al.* (66) also observed substantially increased fibrosis in Cygb KO mice, mostly in the liver, and also in the kidney, suggesting an antifibrotic role of Cygb. Similarly, Mimura *et al.* (42) and Nishi *et al.* (49) used

Cygb-overexpressing transgenic rats in disease models of remnant kidney and renal ischemia/reperfusion, respectively, to provide evidence for an antifibrotic role of Cygb in kidney fibroblasts, potentially *via* a reactive oxygen species (ROS) scavenging function. Despite these investigations, the pathophysiological role of Cygb in the kidney, particularly in cell types other than interstitial fibroblasts, remains poorly understood.

Glomerular visceral epithelial cells, namely podocytes, are highly specialized cells in the Bowman's capsule of the kidney that actively participate in the glomerular filtration process due to their foot processes and slit diaphragm. Podocyte injury is the primary cause of impaired glomerular filtration. Accumulating evidence exists that oxidative stress plays a key role in most pathogenic pathways leading to podocyte defects, for example, observed in diabetic nephropathy (DN) (19). Free radicals such as superoxide can induce cell and tissue injuries through lipid peroxidation, activation of NF- κ B (23), production of peroxynitrite, and induction of apoptosis. Furthermore, ROS and other free radicals can directly induce cell injury. *In vitro* studies indicated that Cygb is able to scavenge free radicals, and overexpression of Cygb in renal immortalized fibroblasts (42, 49) as well as in various other cellular models preserves cell viability under conditions of oxidative stress (12, 26, 33, 61, 74), but the role of Cygb in podocytes remains unexplored.

In the current study, we used a Cygb KO model to investigate the renal function of Cygb and observed a podocyte-associated phenotype. Using cellular models of human podocytes for mechanistic studies, we demonstrated abundant CYGB expression in podocytes and investigated the antioxidative role of CYGB in human podocyte cell lines. Podocytes lacking CYGB displayed increased ROS accumulation and cell death, as well as altered expression of genes involved in the antioxidant defense system and apoptosis. Moreover, human renal biopsy expression data from chronic kidney disease (CKD) patients indicated an association between CYGB and advanced-stage renal disease.

Results

Cygb-deficient mice display reduced kidney function and reduced podocyte number

To analyze the renal expression pattern of Cygb, we performed immunofluorescence analysis on mouse kidney tissue. Immunofluorescence revealed that Cygb is expressed in interstitial fibroblasts as well as in the glomerulus (Fig. 1A). To assess a potential Cygb-dependent effect on kidney function, we used a previously established *Cygb* KO mouse model (65). Reduced Cygb expression in *Cygb*^{-/-} mice was confirmed in whole-kidney mRNA and protein extracts (Fig. 1B, C) as well as on the immunofluorescence level (Fig. 1A). Compared with wild-type mice, *Cygb*^{-/-} mice demonstrated a substantial reduction in renal function, as indicated by an increased serum fluorescein isothiocyanate (FITC)-sinistrin concentration and decreased clearance (Fig. 1D). However, analysis of plasma and urine electrolytes did not show significant differences between the two groups (Supplementary Fig. S1A, B). We also did not observe changes in marker genes of fibrosis and vasculature in whole-kidney RNA (Supplementary Fig. S2A). As we detected Cygb expression in the glomerulus, we next investigated a

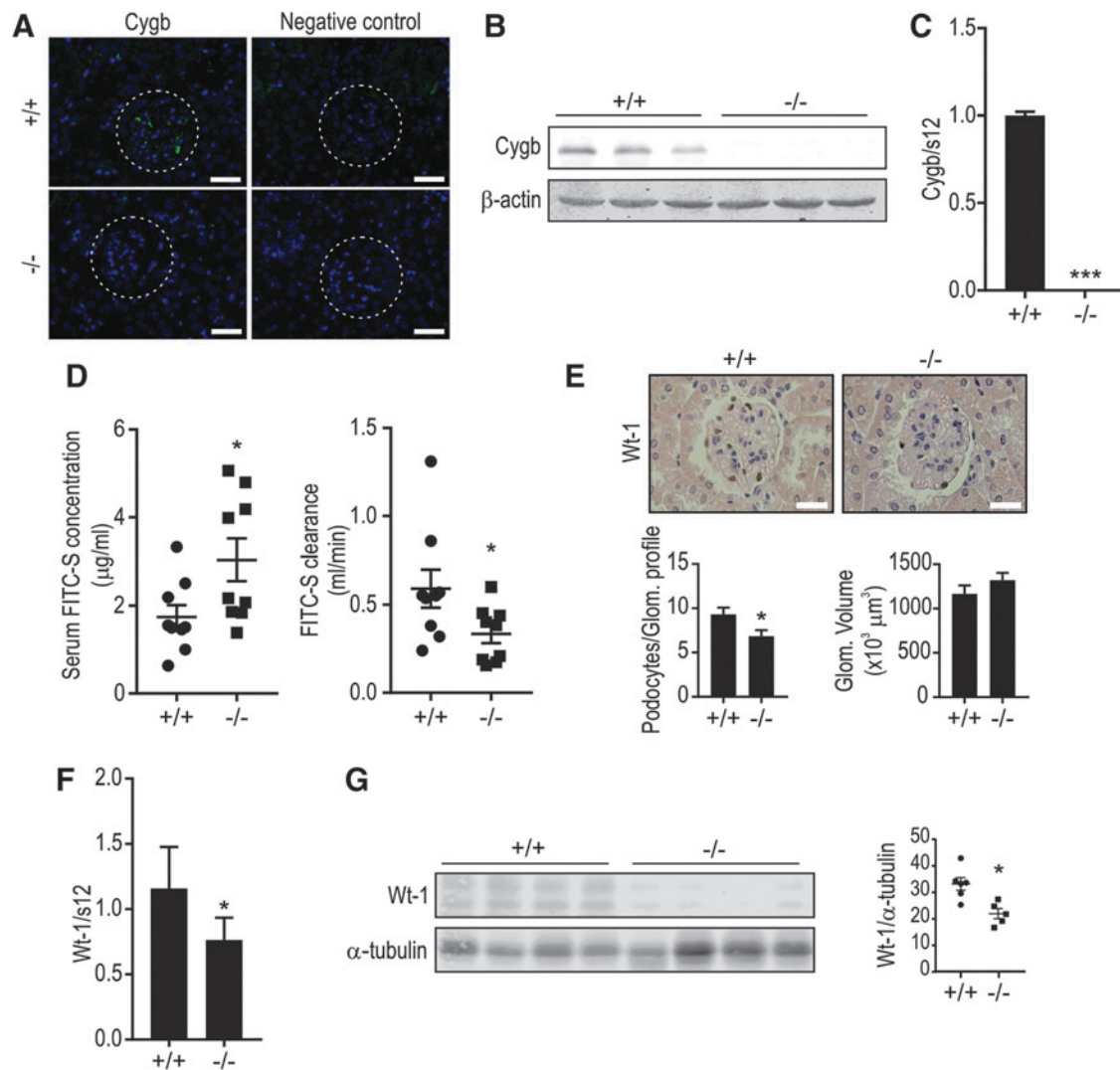


FIG. 1. Cygb deficiency alters kidney function. (A) Immunofluorescence detection of Cygb in WT ($Cygb^{+/+}$) and KO ($Cygb^{-/-}$) mice. Incubation without primary antibody served as negative control (scale bar $100\ \mu\text{m}$). Dashed white circle indicates glomerular region. Green: Cygb, blue: DAPI. (B) RNA and (C) protein levels of Cygb in $Cygb^{+/+}$ and $Cygb^{-/-}$ mice. β -Actin was used as loading control. $***p < 0.001$. (D) Serum FITC-sinistrin (FITC-S) concentration and clearance in $Cygb^{+/+}$ and $Cygb^{-/-}$ mice at baseline conditions. Results are indicated as mean \pm SEM of $n = 9$ for each group. $*p < 0.05$; Student's *t*-test. (E) Wt-1 immunostaining in $Cygb^{+/+}$ and $Cygb^{-/-}$ mice (scale bar $20\ \mu\text{m}$). Average number of Wt-1-positive nuclei (bottom left) and average glomerular volume (bottom right) in the two groups. Results are indicated as mean \pm SEM of $n = 5$ mice for each group. $*p < 0.05$; Student's *t*-test. (F) RNA and (G) protein levels of Wt-1 with corresponding protein quantification. α -Tubulin was used as loading control. $*p < 0.05$; Student's *t*-test. CYGB/Cygb, human/mouse cytoglobin; DAPI, 4',6-diamidino-2-phenylindole; FITC, fluorescein isothiocyanate; SEM, standard error of mean.

potential role of podocytes in this phenotype. The average number of podocytes per glomerular cross section was determined by counting cells stained with the podocyte-specific marker Wt-1 (20). Although no apparent difference in proteinuria (Supplementary Fig. S1F) nor clear gross morphological kidney changes were observed in the two groups (Supplementary Fig. S1G), podocyte numbers were significantly reduced in $Cygb^{-/-}$ mice compared with $Cygb^{+/+}$ mice, as assessed by immunohistochemistry (Fig. 1E). Consistent with this observation, Wt-1 mRNA (Fig. 1F) as well as protein levels (Fig. 1G) were downregulated in $Cygb^{-/-}$ mice, confirming a decreased podocyte number.

Abundant CYGB expression in podocyte cell models

To mechanistically investigate the role of CYGB in the glomerulus, we explored CYGB levels in human podocyte cell culture models. Compared with various human kidney-derived cell lines, including proximal tubule cells, fibroblasts, and embryonic cells, the most abundant endogenous CYGB mRNA and protein levels were observed in podocytes, particularly in AB8/13 (Fig. 2A), which was used for subsequent investigations. The heat-sensitive AB8/13 cells proliferate at the permissive temperature of 33°C , and stop proliferating and undergo differentiation within 2 weeks

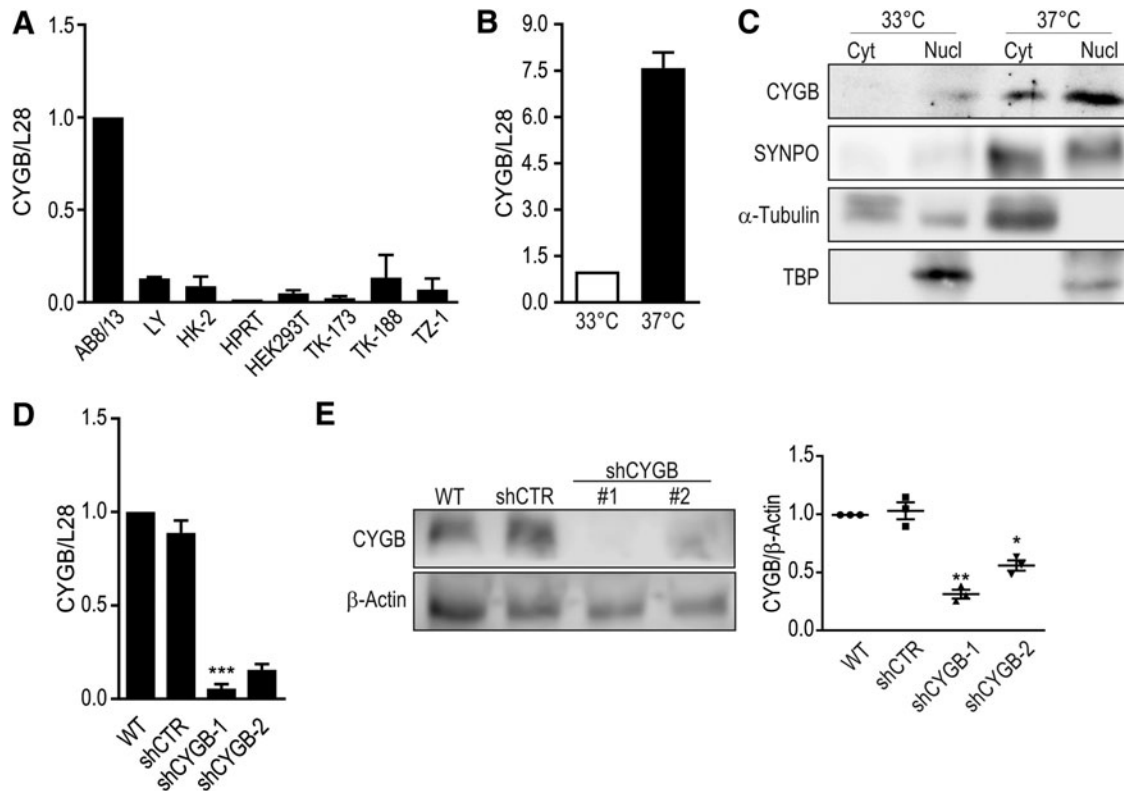


FIG. 2. AB8/13 cells express abundant CYGB mRNA levels. (A) CYGB mRNA expression in human kidney-derived cell lines. HK-2 and HPRT, proximal tubule cell lines; HEK293T, embryonic kidney; TK-173, TK-188, and TZ-1, fibroblasts; LY and AB8/13, podocytes ($n=4$) (B) CYGB mRNA expression and (C) CYGB protein levels in AB8/13 before (33°C) and after 10–14 days of differentiation at 37°C. Cyt, cytoplasmic fraction; Nucl, nuclear fraction. SYNPO was used as marker of differentiated podocytes, α -tubulin as cytoplasmic marker, and TBP as nuclear marker. (D) Stable CYGB knockdown with two independent shRNA constructs (shCYGB-1, shCYGB-2) was confirmed on the mRNA level ($n=4$). *** $p < 0.001$ compared with WT; one-way ANOVA and Tukey correction for multiple comparisons. (E) Representative immunoblot (left panel) and densitometry analysis (right panel) of CYGB knockdown cells. β -Actin was used as loading control. * $p < 0.05$; ** $p < 0.01$; compared with WT; one-way ANOVA and Tukey correction for multiple comparisons. ANOVA, analysis of variance; shRNA, short hairpin RNA; TBP, TATA-box binding protein.

at the nonpermissive temperature of 37°C (57). Reverse transcription-quantitative polymerase chain reaction (RT-qPCR) revealed that CYGB mRNA is differently expressed before and after podocyte differentiation (Fig. 2B), and the CYGB protein is localized in both the cytoplasm and nucleus, as assessed by immunoblotting (Fig. 2C).

We established stable AB8/13 knockdown cells using two independent short hairpin RNA (shRNA) sequences targeting CYGB, termed shCYGB-1 and shCYGB-2. CYGB knockdown efficiency was confirmed at the mRNA and protein level (Fig. 2D, E). To obtain an independent podocyte cell culture model, we also generated stably CYGB-depleted shRNA LY cells (Supplementary Fig. S3).

Antiapoptotic role of CYGB in AB8/13

A putative antiapoptotic role of CYGB has been suggested in some cell lines (60, 67), but not in podocytes. This prompted us to investigate cell viability in our cell models. CYGB knockdown podocyte cell lines displayed increased cell death (Fig. 3A), indicating a role of CYGB in cell survival. A similar reduction in cell viability was observed in the independently analyzed LY podocyte cell line (Supplementary Fig. S2). Consistently, we observed substantially in-

creased cleaved-PARP1 levels in shCYGB-1 cells (Fig. 3B), but not in shCYGB-2, possibly due to its more moderate knockdown of CYGB. Moreover, MTT assays demonstrated that shCYGB-1 cells were more susceptible to H₂O₂ and antimycin A (AMA) compared with WT and shCTR cells (data not shown). Terminal deoxynucleotidyl transferase dUTP nick end labeling (TUNEL) assays revealed DNA double-strand breaks in shCYGB-1 and shCYGB-2 cells treated with H₂O₂ for 3 h, but not in shCTR cells (Fig. 3C).

Due to the intimate link between cell death and mitochondrial functions (ATP production and apoptosis), we investigated a potential CYGB-dependent effect on the bioenergetic status in AB8/13 cells. For this purpose, we analyzed mitochondrial respiration, measured as oxygen consumption rate (OCR). Cells were treated sequentially with oligomycin, carbonyl cyanide-4 trifluoromethoxy phenylhydrazone (FCCP), and rotenone/AMA to challenge the mitochondrial electron transport chain and evaluate possible differences in OCR response. CYGB downregulation was associated with decreased OCR already at baseline and also following addition of the various mitochondrial stressors (Fig. 3D). The lower OCR after oligomycin in shCYGB-1 cells is linked to lower ATP production compared with

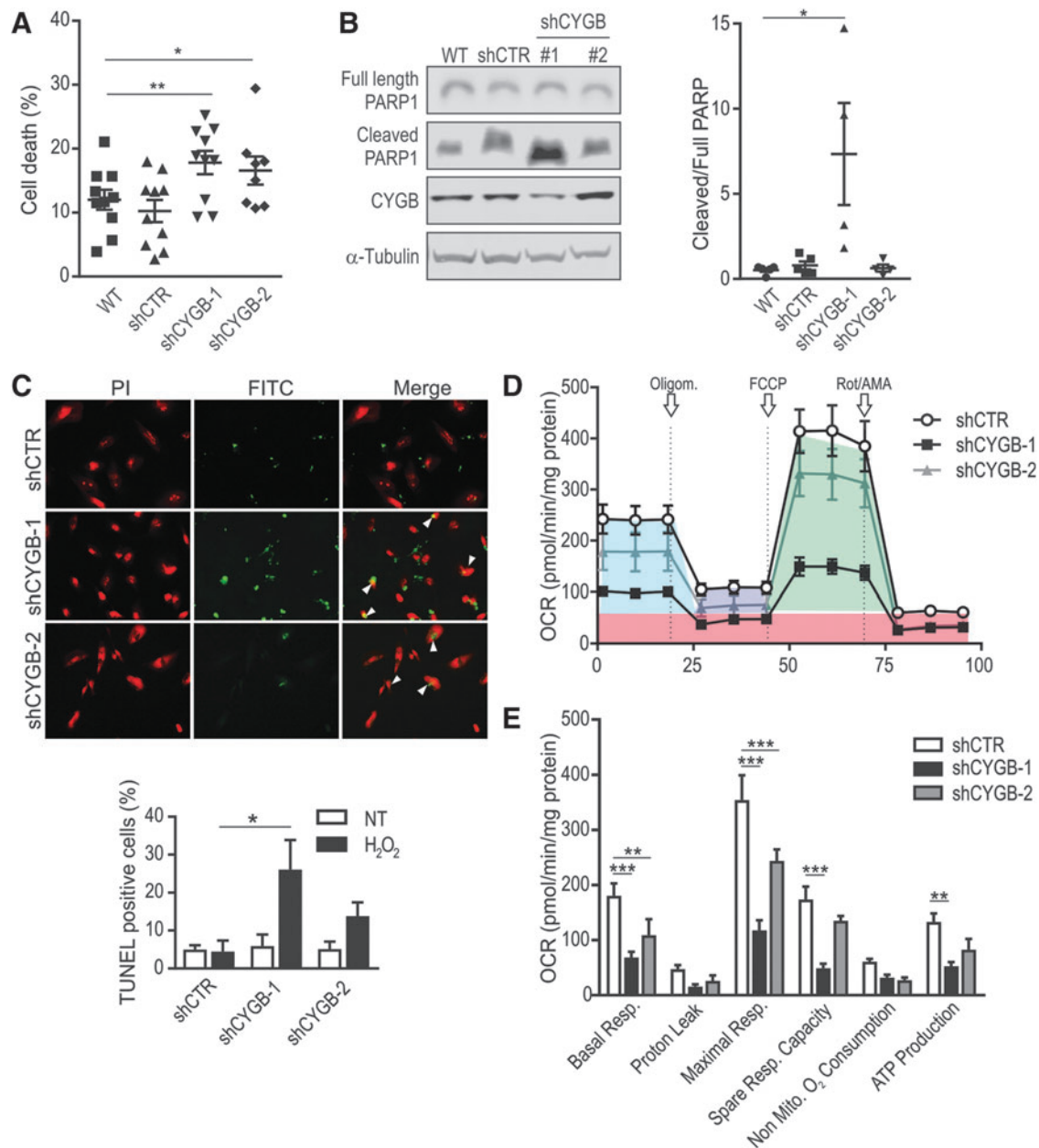


FIG. 3. CYGB protects against cell death and apoptosis. (A) Cell death was measured by trypan blue exclusion ($n=8-10$). $*p < 0.05$, $**p < 0.01$; one-way ANOVA and Tukey correction for multiple comparisons. (B) Representative immunoblot displaying PARP1 cleavage in CYGB knockdown cells compared with WT and shCTR (left panel) and densitometry analysis (right panel). α -Tubulin was used as loading control. (C) TUNEL assay (FITC, Green) in shCTR, shCYGB-1, and shCYGB-2 cells following H_2O_2 treatment (top panel) and corresponding quantification of TUNEL-positive cells (bottom panel). Arrowheads indicate TUNEL-positive staining. $*p < 0.05$; two-way ANOVA and Sidak's correction for multiple comparisons. (D) OCR in shCTR, shCYGB-1, and shCYGB-2 cells with arrows indicating sequential injections into media of the specific stressors oligomycin (Oligom.), FCCP, and Rot/AMA, normalized by protein content. Red, nonmitochondrial respiration; blue, basal respiration; purple, proton leak; green, maximal respiration. (E) Comparison of different mitochondrial parameters calculated from the OCR profile in shCTR, shCYGB-1, and shCYGB-2 cells ($n=4$). $***p < 0.001$; $**p < 0.01$; two-way ANOVA and Dunnett's multiple comparisons test. AMA, antimycin A; FCCP, carbonyl cyanide-4 trifluoromethoxy phenylhydrazone; OCR, oxygen consumption rate; PI, propidium iodide; Rot, rotenone; TUNEL, terminal deoxynucleotidyl transferase dUTP nick end labeling.

shCTR, consistent with a decreased mitochondrial activity. Subsequent FCCP treatment resulted in an increased maximal OCR in shCTR cells compared with CYGB knockdown cells. Until this stage, shCYGB-2 cells (characterized by a less pronounced knockdown of CYGB than shCYGB-1

cells, Fig. 2E) displayed an intermediate phenotype between shCTR and shCYGB-1. However, after the final treatment with rotenone and AMA, shCYGB-1 and -2 cells reached the same minimal OCR, while shCTR cells displayed higher levels, suggesting a higher nonmitochondrial

respiration in control cells compared with CYGB knock-down podocytes (Fig. 3E). Overall, these data indicate that CYGB supports podocyte viability by preserving mitochondrial bioenergetics.

Antioxidative role of CYGB in AB8/13

To further investigate the putative antioxidative role of CYGB in podocytes, we analyzed expression levels of the redox-sensitive genes heme oxygenase 1 (*HO-1*) and *HSP1A1*. Basal mRNA levels of both *HO-1* and *HSP1A1* were increased in shCYGB-1 cells compared with WT and shCTR cells (Supplementary Fig. S4), indicating a CYGB-dependent altered intracellular redox state. Similarly, *HO-1* expression levels were increased in CYGB-depleted LY podocytes (Supplementary Fig. S2). To further confirm this observation, WT, shCTR, and shCYGB AB8/13 cells were transiently transfected with the cytoplasmic oxidation-sensitive roGFP2-Orp1 probe. Compared with WT cells, shCYGB-1 and shCYGB-2 cells showed a significant increase in roGFP2-Orp1 oxidation under basal conditions (Fig. 4A), consistent with the gene expression data. Treatment with AMA, a mitochondrial complex III inhibitor,

further increased roGFP2-Orp1 oxidation, particularly in the two shCYGB cell models (Fig. 4A). As an independent approach to measure ROS generation in podocytes, we used 2',7'-dichlorodihydrofluorescein diacetate (H₂DCFDA), a fluorescent cell-permeable indicator of ROS. Immediately after AMA treatment, 2',7'-dichlorofluorescein (DCF) fluorescence strongly increased in shCYGB-1 cells compared with WT and shCTR cells (Fig. 4B). To confirm the results with an independent ROS stimulus, cells were subjected to 250 μ M H₂O₂, and DCF fluorescence was measured over a 4-h period. ROS accumulation rapidly increased in shCYGB-1 and shCYGB-2 cells, reaching the highest value after 4 h (Fig. 4C).

Since podocyte loss has been associated with hyperglycemia and subsequent increase in oxidative stress (63), cells were incubated with high glucose (HG) or mannitol (used as iso-osmotic control) for 5 days. Treatment with HG significantly increased ROS accumulation (Fig. 4D) and cell death (Fig. 4E) in shCYGB-1 and shCYGB-2 cells compared with WT cells, indicating a protective role of CYGB in oxidative stress-mediated cell death. On the contrary, overexpression of CYGB reduced ROS accumulation and oxidative stress as assessed by roGFP2-Orp1 oxidation and H₂DCFDA-based

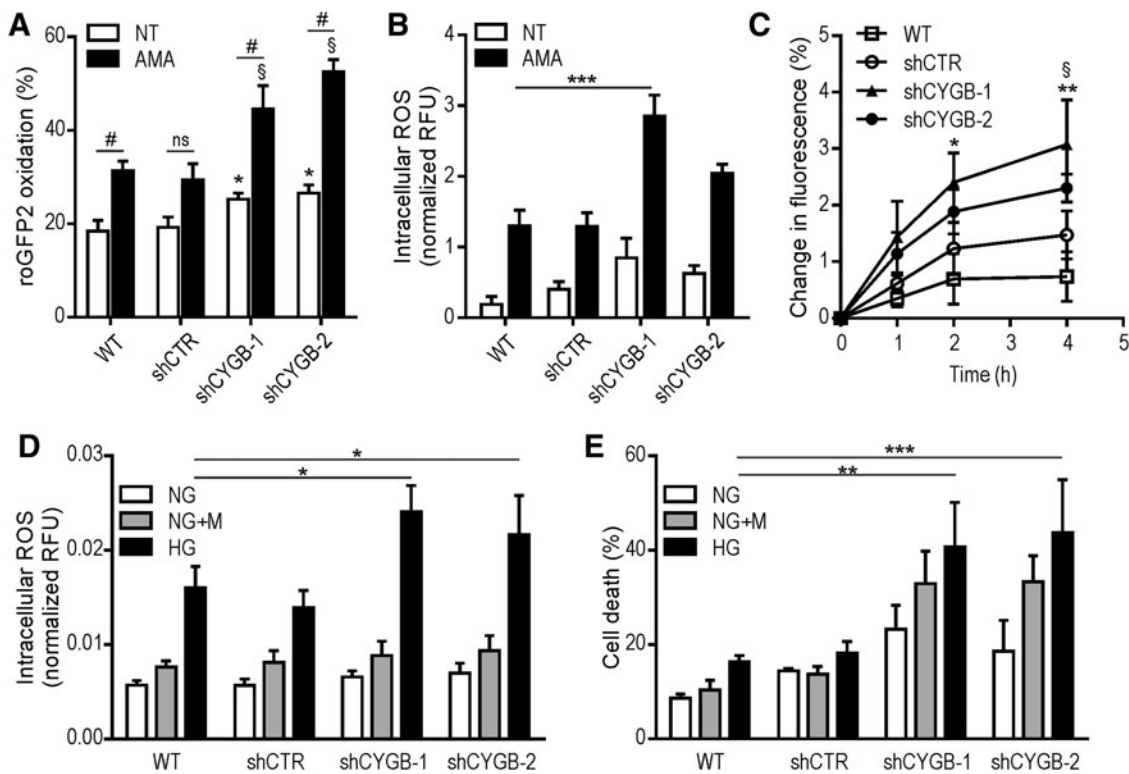


FIG. 4. CYGB deficiency causes oxidative stress. (A) Oxidation of the cytoplasmic redox-sensitive probe roGFP2-Orp1 in WT, shCTR, shCYGB-1, and shCYGB-2 cells under nontreated conditions (NT) and upon AMA treatment ($n=4$). $*p < 0.05$; Student's *t* test compared with NT WT cells; $§p < 0.05$; compared with AMA WT; $\#p < 0.001$; ns, nonsignificant; two-way ANOVA and Tukey's *post hoc* test. (B) Intracellular ROS production following AMA treatment ($n=3$). $***p < 0.001$; two-way ANOVA and Tukey's *post hoc* test compared with WT and shCTR cells. (C) Kinetics of H₂O₂ treatment in WT, shCTR, shCYGB-1, and shCYGB-2 cells $*p < 0.05$; $**p < 0.01$ (shCYGB-1 compared with WT); $§p < 0.05$ (shCYGB-2 compared with WT); two-way ANOVA and Tukey's *post hoc* test. ($n=4-6$). (D) ROS accumulation in WT, shCTR, shCYGB-1, and shCYGB-2 cells upon normal (NG) or high (HG) glucose treatment. Mannitol (NG + M) was used as osmotic control ($n=4$). (E) Cell death quantification (trypan blue exclusion method) of WT, shCTR, shCYGB-1, and shCYGB-2 cells subjected to NG or HG glucose treatment. Mannitol (NG + M) was used as osmotic control ($n=4$). $*p < 0.05$; $**p < 0.01$; $***p < 0.001$; two-way ANOVA and Tukey's *post hoc* test. ROS, reactive oxygen species.

assays upon different stimuli (Supplementary Fig. S5). Collectively, these data provide evidence for an antioxidative role of CYGB in podocytes.

CYGB deficiency alters expression of multiple genes involved in redox signaling and apoptosis

The CYGB-dependent transcriptome was determined by RNA sequencing of shCTR and shCYGB-1 cells. Three independent samples for each condition were analyzed and the knockdown efficiency of shCYGB-1 was confirmed to be >90% (Supplementary Fig. S6A). Most of the total reads mapped to exons (90%), whereas introns and intergenic regions accounted only for 9% and 1% of the total reads, respectively (Supplementary Fig. S6B), confirming the quality of the multiple mapping. Furthermore, sample-to-sample distance and principal component analysis (PCA) of the RNA-seq data sets indicate clear separation among shCYGB and shCTR cells (Supplementary Fig. S6C, D).

To ascertain the reliability of the sequenced samples, the transcriptomic data were compared with podocyte-specific marker genes based on literature search and single-cell RNA sequencing (scRNA-seq) (39). Genes were considered to be expressed in the shCTR and shCYGB AB8/13 data sets if the mean reads per kilobase per million mapped reads (RPKM) value were ≥ 0.1 and ≥ 0.5 , respectively (39). In shCTR AB8/13 cells, 83%–95% of the literature-based (RPKM $\geq 0.5 = 68/82$; RPKM $\geq 0.1 = 72/82$) and 76%–82% of the scRNA-seq-based (RPKM $\geq 0.5 = 58/76$; RPKM $\geq 0.1 = 62/76$) essential podocyte genes were expressed (Supplementary Tables S1 and S2), thereby validating that AB8/13 cells represent a genuine podocyte model.

More than 1500 genes were found differentially expressed in shCYGB compared with shCTR cells (Fig. 5A), and among these, the majority (1148) was downregulated. The most significantly upregulated genes included ubiquitin D (*UBD*), UDP glucuronosyltransferase family 1 member A6 (*UGT1A6*), and neuropeptide Y receptor Y4 (*NPY4R*), whereas the most significantly downregulated genes included activity regulated cytoskeleton associated protein (*ARC*), heparan sulfate 6-*O*-sulfotransferase 2 (*HS6ST2*), and MAF BZIP transcription factor B (*MAFB*). To investigate if the observed differentially expressed genes are associated with common canonical pathways based on established interactions among them, an ingenuity pathway analysis (IPA) was carried out. Interestingly, differentially expressed genes could be attributed to multiple kidney failure-associated pathways (Supplementary Table S3). In addition, using the CLC Genomics Workbench 8.5.1 RT² Profiler gene lists (Qiagen), we observed an association of the CYGB-dependent transcriptome with apoptosis and oxidative stress pathways (Supplementary Table S4). Using similar RT² Profiler gene lists as well as Gene Ontology (GO), Kyoto Encyclopedia of Genes and Genomes (KEGG), and IPA tools, we also specifically looked at metabolism-associated genes, but no clear enrichments could be observed (data not shown). Furthermore, analysis of expression levels of candidate metabolism-associated genes in whole-kidney extracts of *Cygb*^{+/+} and *Cygb*^{-/-} mice did not reveal any apparent differential regulation *in vivo* (Supplementary Fig. S1E).

In line with the increased oxidative stress and apoptosis of CYGB-depleted AB8/13 cells, several antioxidant genes

such as *DUOX-1*, *DUOX-2*, and *GPX-3*, as well as some antiapoptotic genes, such as *TP73*, were found to be downregulated. Furthermore, multiple genes indicating podocyte injury, including *SERPINE1* and *CTGF*, were upregulated (Table 1). To validate the most relevant differentially expressed genes, we performed RT-qPCR on independent RNA samples of shCYGB and shCTR AB8/13 cells (Fig. 5B). A similar CYGB-dependent regulation of *DUOX-1*, *GPX-3*, and *SOD3* was found in LY cells, validating the results observed in AB8/31 (Fig. 5C). In contrast, a selection of redox-sensitive genes were not differentially regulated in whole-kidney lysates of *Cygb*^{+/+} and *Cygb*^{-/-} mice (Supplementary Fig. S1F). Consistently, levels of protein carbonyls in whole-kidney lysates from *Cygb*^{+/+} and *Cygb*^{-/-} mice were comparable, suggesting the absence of apparent differences in ROS levels *in vivo* (Supplementary Fig. S1G). Of particular interest is the downregulation of WT-1 and MAFB, both established regulators of podocyte development and viability in shCYGB AB8/13 cells *versus* shCTR cells. A similar, although less pronounced, downregulation of WT-1 and MAFB could be observed in stably CYGB-depleted LY cells (Fig. 5C). To confirm this CYGB-dependent regulation on protein level, we carried out immunoblotting for both proteins. Immunoblotting experiments clearly recapitulated the obtained RNA results, illustrating reduced protein expression of WT-1 and MAFB in CYGB-deficient AB8/13 cells compared with shCTR cells (Fig. 5D). A comparable trend could be observed in CYGB-deficient LY cells (Fig. 5E). Finally, we also evaluated MafB expression levels in whole-kidney lysates of *Cygb*^{+/+} and *Cygb*^{-/-} mice, demonstrating reduced renal MafB mRNA and protein levels in *Cygb*-deficient mice (Supplementary Fig. S2B, C). Collectively, analysis of the CYGB-dependent transcriptome in AB8/13 cells revealed altered expression of multiple genes involved in redox signaling and apoptosis as well as essential factors of podocyte biology, consistent with the CYGB-dependent phenotype.

CYGB is associated with CKD

Genome-wide association studies (GWAS) have proven to be a powerful tool in identifying novel genetic markers involved in CKD (50). By using GWAS databases (3), we identified a single-nucleotide polymorphism (SNP), located in an intergenic region 3' of the *CYGB* gene associated with albuminuria (Fig. 6A). University of California Santa Cruz-integrated ENCODE data (10) illustrate that the SNP (rs8082416) is localized in a DNaseI hypersensitivity cluster observed in 115 cell types that reflects open chromatin, and overlaps with strong transcription factor occupancy (Supplementary Fig. S7A). Chromatin immunoprecipitation-sequencing data sets further revealed histone marks for an active enhancer (H3K4Me1) and basal components of the transcriptional machinery (RNA pol2 in cell lines SK-N-MC, IMR90, and HCT-116; as well as p300 in H1-hESC) in this region. In addition, RNA polymerase II-associated chromatin interaction analysis by paired-end tag (ChIA-PET) sequencing data in MCF-7 cells from ENCODE suggested DNA looping of this potential enhancer region to the first intron of the *CYGB* gene, close to its transcription initiation site. To experimentally validate a putative synergistic action between this potential 3'-enhancer and the *CYGB* promoter, we performed luciferase reporter gene assays. Whereas a

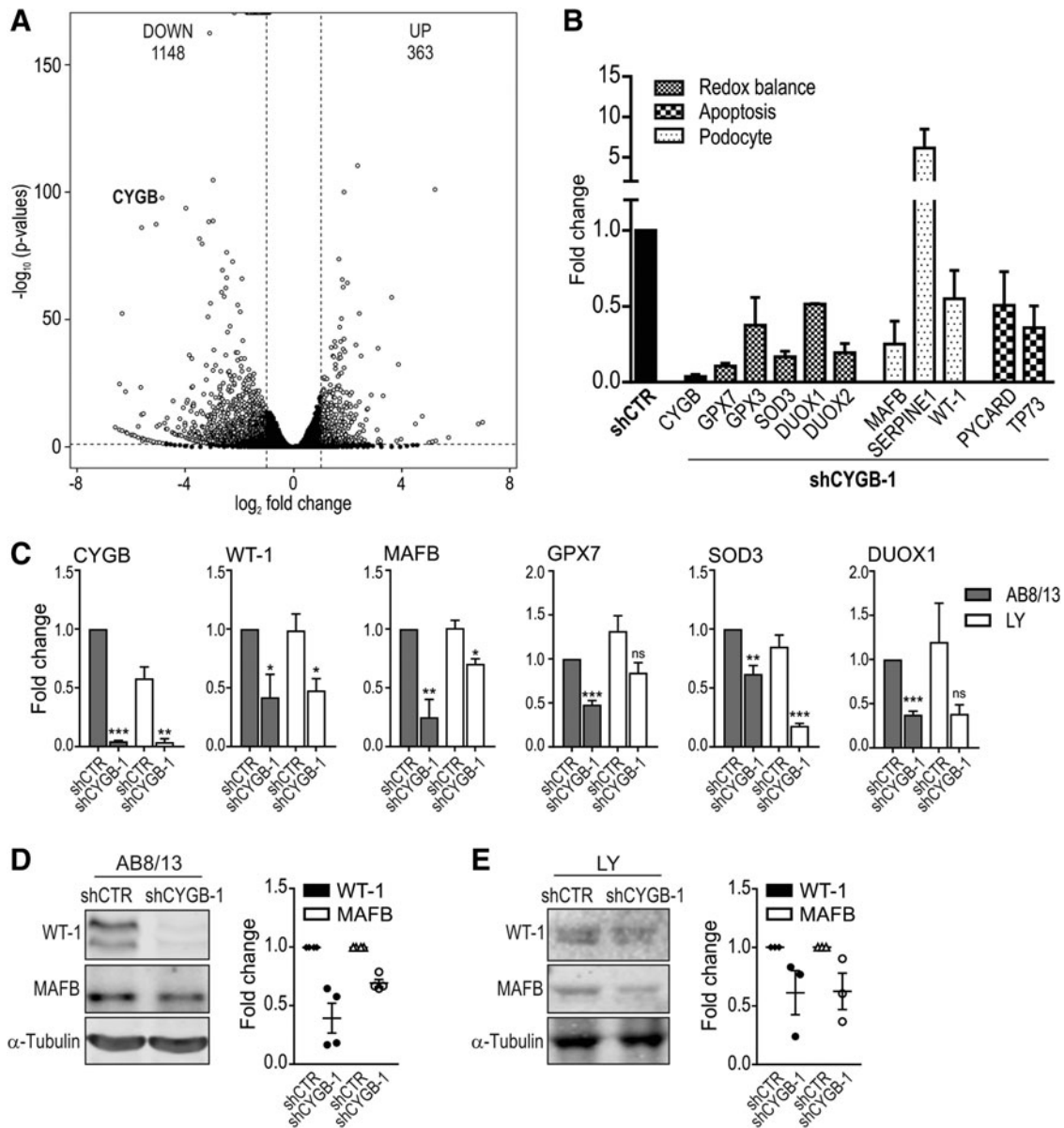


FIG. 5. CYGB knockdown alters expression of genes involved in redox balance and podocyte phenotype maintenance. (A) Volcano plot showing the distribution of differentially expressed genes following CYGB knockdown. *White dots*, $|\text{Fold change}| > 2$, $p < 0.05$; *black dots*, $|\text{Fold change}| < 2$, not significant. (B) Validation of the results by reverse transcription-quantitative polymerase chain reaction on independent RNA samples. (C) Validation of selected genes downregulated in an independent podocyte cell line (LY), in comparison with AB8/13 ($n = 4$). * $p < 0.05$; ** $p < 0.01$; *** $p < 0.001$; Student's *t*-test. (D, E) Representative immunoblot showing downregulation of two specific podocyte markers (MAFB and WT-1) in (D) AB8/13 cells and (E) in LY cells and corresponding quantification. α -Tubulin was used as loading control.

90 bp fragment of the 3'-enhancer spanning the SNP did not regulate heterologous SV40 promoter-driven luciferase activity, the 3'-enhancer substantially increased endogenous CYGB promoter-driven luciferase activity (Supplementary Fig. S7B), confirming a cooperation between the downstream enhancer and the CYGB promoter. However, the SNP site did not directly alter the transcriptional activity of the CYGB gene under basal conditions as no change in luciferase activity could be observed between the WT and mutated 3'-enhancer-driven construct (Supplementary Fig. S7B).

As an independent approach, existing gene array data from human renal biopsy specimens collected from the European Renal cDNA Bank (8) were analyzed. Data were obtained from Affymetrix HG-U133 Plus 2.0 microarrays, hybridized with glomerular and tubulointerstitial complementary DNA (cDNA) procured from different nephropathies as well as pretransplant biopsies from living renal allograft donors as controls. These biopsy expression studies from CKD patients revealed a consistent association of CYGB expression levels with advanced end-stage CKD, including DN (Fig. 6B).

TABLE 1. LIST OF DIFFERENTIALLY EXPRESSED GENES IN SHCYGB-1 COMPARED WITH SHCTR CELLS

Function	Gene ID	Fold change	p-Value
Antioxidant	<i>CYGB</i>	-28.92	1.1E-98
Antioxidant	<i>SOD3</i>	-3.70	8.0E-04
Antioxidant	<i>GPX3</i>	-4.69	9.97E-19
Antioxidant	<i>GPX7</i>	-2.96	4.8E-03
Antioxidant	<i>DUOX-1</i>	-18.14	3.3E-05
Antioxidant	<i>DUOX-2</i>	-12.40	3.8E-07
Podocyte phenotype	<i>MAFB</i>	-86.20	1.8E-25
Podocyte phenotype	<i>WT-1</i>	-2.26	4.1E-02
Podocyte injury	<i>SERPINE1</i>	2.19	1.87E-27
Apoptosis	<i>PYCARD</i>	-2.73	2.7E-06
Apoptosis	<i>TP73</i>	-2.45	2.05E-08

Genes are divided in four categories: antioxidant, podocyte phenotype, podocyte injury, and apoptosis. *p*-Values are corrected for multiple statistical testing by FDR.

FDR, false discovery rate.

CYGB mRNA levels in different kidney diseases were validated by RT-qPCR in an independent patient cohort, supporting the association of increased CYGB mRNA levels with DN (Fig. 6C). In summary, these data suggest an association of CYGB with CKD.

Discussion

Based on *in vivo* and *in vitro* data, we propose that Cygb has a previously underappreciated role in podocyte function. Our study demonstrates that *Cygb* is expressed in mouse glomeruli, is important to preserve basal renal function possibly *via* a podocyte-related role, and can protect podocytes from oxidative stress and cell death under various experimental conditions *in vitro*. Specifically, CYGB-deficient

podocytes display increased ROS accumulation and apoptosis, as well as dysregulation of multiple genes involved in cellular redox balance, apoptosis, and podocyte integrity. In addition, we provide evidence for an association of CYGB with CKD using patient biopsies.

Whereas the antioxidative function of CYGB has reached a consensus in the globin field, the precise molecular mechanism underlying this function is still poorly understood. Most likely CYGB may scavenge ROS using heme and thiol residues (13, 51), while peroxidase and superoxide dismutase activity has been excluded by the investigations of Trandafir *et al.* (68). In an attempt to investigate the molecular mechanism in more depth, we explored the function of CYGB in various renal cell models. To the best of our knowledge, a role of CYGB in podocytes has not been investigated so far.

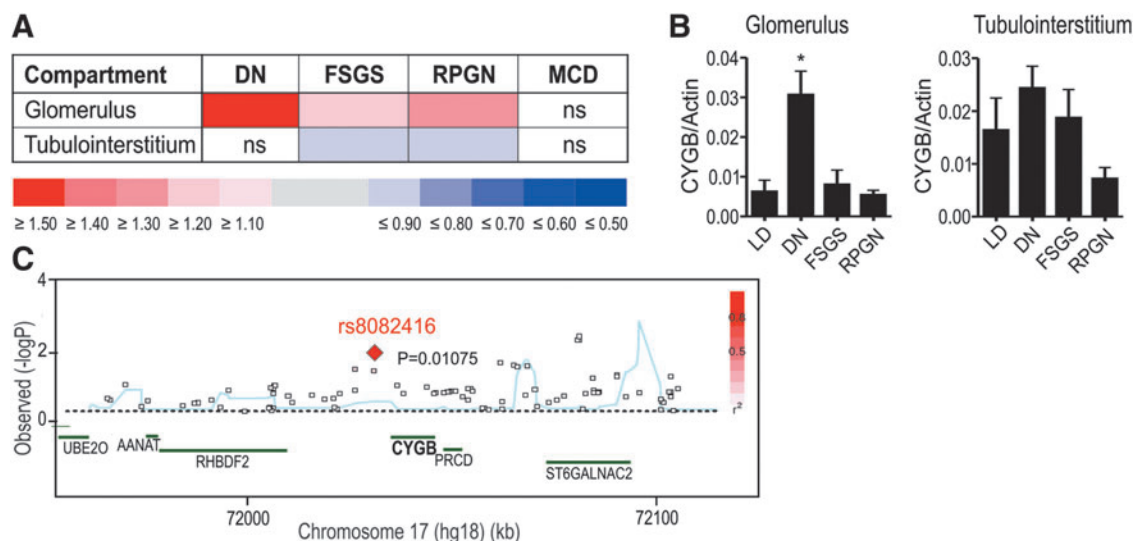


FIG. 6. Association of *CYGB* with CKD. (A) Regional association plot for the *CYGB* gene region displaying a single-nucleotide polymorphism associated with CKD obtained from a genome-wide association study (3). $\log_{10} p$ -values are plotted versus genomic position, using gene annotations obtained from the University of California Santa Cruz Genome Browser (RefSeq Genes, build 36). (B) Gene expression data of microdissected glomeruli and tubulointerstitial compartments from patients with glomerulopathies. Values are log fold changes relative to LD. * $p < 0.05$. (C) *CYGB* mRNA levels were validated in an independent cohort of microdissected samples by reverse transcription-polymerase chain reaction and normalized to β -actin mRNA levels. CKD, chronic kidney disease; DN, diabetic nephropathy; FSGS, focal segmental glomerulosclerosis; LD, living donors; MCD, minimal change disease; RPGN, rapidly progressive glomerulonephritis.

Consistent with the RNA-sequencing-based results of microdissected renal tubules from Lee *et al.* (32), the studies by Geuens *et al.* (18), and the recent results of Balkawade *et al.* (1), we detected high levels of *Cygb* protein in mouse glomeruli (Fig. 1A). *Cygb*-deficient mice displayed a reduced number of podocytes (Fig. 1E). Consistently, renal function, as measured by FITC-sinistrin clearance, was reduced in *Cygb*-deficient mice (Fig. 1D). Mechanistic studies in two cellular models of podocytes, which express more abundant endogenous CYGB levels compared with any other kidney-derived cell lines (Fig. 2A), validate an antioxidative function of CYGB. CYGB depletion, using independent shRNA targeting sequences (Fig. 2D, E), induced increased cell death as measured by trypan blue exclusion (Fig. 3A) and cleaved PARP (Fig. 3B), an established apoptosis marker as well as DNA damage (Fig. 3C), corroborating with the previously observed antiapoptotic role of CYGB (14, 31, 60, 61). Using complementary methods, we show that podocytes with attenuated CYGB expression display increased oxidative stress (Fig. 4A–E). In line with this observation, analysis of cellular bioenergetics suggest impaired mitochondrial function in CYGB depleted cells as evidenced by reduced mitochondrial respiratory capacity (Fig. 3D, E). An NO dioxygenase function has been suggested for CYGB (17, 24). As AB8/13 cells only express very low levels of NO synthases, an NO-mediated inhibiting effect of basal OCR, following knock-down of CYGB, is very unlikely and rather argues for an ROS-dependent effect of altered mitochondrial respiratory capacity. CYGB overexpression on the contrary reduced oxidative stress, prevented ROS accumulation in AMA-treated podocytes, and promoted cell viability, in line with previous findings (14, 26, 74). Podocyte apoptosis has been demonstrated as a cause of podocyte depletion (30). Similar to the phenotype of reduced number of podocytes observed in our *Cygb*^{-/-} mice, multiple pathologies such as DN have been associated with loss of podocytes. Specifically, in DN, hyperglycemia-induced ROS accumulation was shown to contribute to podocyte apoptosis and depletion (35, 63). Upon treatment with HG, CYGB-deficient podocyte cells displayed increased ROS production and more pronounced cell death, compared with controls, strongly suggesting a protective role of CYGB. In contrast to our expectations, we did not observe albuminuria or proteinuria in *Cygb*^{-/-} mice. Accordingly, MacIsaac *et al.* reported that the absence of proteinuria does not preclude loss of renal function (41). Alternatively, this lack might be due to the mild nature of the *Cygb* phenotype that, despite decreased podocyte number, is able to maintain filter barrier integrity or, in case it is not, may rely on enhanced proximal tubule endocytic activity resulting in compensating proximal tubular protein reabsorption. In support of the latter hypothesis, increased megalin expression has recently been described in type 2 diabetes (4). Future studies are required to study if challenging conditions such as induction of DN would lead to proteinuria in *Cygb*^{-/-} mice. According to the study of Susztak *et al.* (63), hyperglycemia-induced overproduction of ROS could cause a diminution of the number of podocytes, which could contribute to the development of DN. Although CYGB knockout was sufficient to induce some histological changes such as podocyte loss, it was not sufficient to induce other histological changes as well as functional changes in the glomerulus (albuminuria). These changes may become apparent upon exposure to diabetic

conditions and suggest a certain threshold of podocyte injury, which is exacerbated under diabetic conditions (2, 53). On the contrary, we cannot exclude a developmental defect in the *Cygb*^{-/-} mice.

Transcriptome analysis of CYGB-deficient podocytes and control cells revealed dysregulation of multiple genes involved in redox balance, apoptosis, podocyte function, and podocyte injury (Fig. 5A, B). Most of the genes were downregulated, indicating a general transcriptional repression in the absence of CYGB. As this could potentially hint to a decreased metabolic function, we performed a close inspection of metabolism-associated genes, but only could observe a few moderate changes in gene expression, insufficient for explaining a decreased metabolic function. Similarly, a decrease in general mRNA stability upon lowered CYGB expression cannot be ruled out.

Due to its homology to Mb and comparable O₂-binding affinity, CYGB was originally thought to contribute to intracellular O₂ supply (69), acting as an O₂ reservoir or as a signal transducer in O₂ sensing pathways (18, 25). Therefore, CYGB deficiency would decrease oxygen availability and ROS signaling. DUOX-1 and DUOX-2 belong to the NADPH oxidase family and need oxygen as cosubstrate to produce ROS (*i.e.*, H₂O₂ or O₂⁻). Both DUOX-1 and DUOX-2 are downregulated in lung cancer (40) and in hepatocellular carcinoma (DUOX-1) (34), in conditions where increased ROS levels were observed. However, their role in podocytes is still unknown. Downregulation of antioxidative genes, including CYGB, SOD3, GPX3, and GPX7, could explain the accumulation of ROS, as previously reported (60). The absence of differential expression of these antioxidative genes in whole-kidney lysates of *Cygb*^{+/+} and *Cygb*^{-/-} mice might be explained by compensation of multiple other surrounding cell types.

Intriguingly, attenuated CYGB expression leads to downregulation of WT-1 and MAFB, essential podocyte transcription factors involved in maintaining cell differentiation (Fig. 5C–E). In line with these *in vitro* data, both *Wt-1* and *MafB* were downregulated in *Cygb*^{-/-} mice. WT-1 represents a key regulator of podocyte function and its downregulation leads to glomerulonephritis and mesangial sclerosis (20). Various mutations in WT-1 cause podocytopathies, including Denys–Drash syndrome, Frasier syndrome, and nonsyndromic focal segmental glomerulosclerosis (FSGS) (43). Whereas major efforts have focused on the identification of transcriptional targets of WT-1 in podocytes, the finding of an upstream regulator is of substantial interest as well. Moreover, WT-1 promotes expression of a large subset of the podocyte proteome, probably by activating the transcription of other transcriptional regulators that act either cooperatively with or independently of WT-1 (43). Studies by Dong *et al.* (11) provided evidence that WT-1 represents a crucial transcription factor for podocyte maturation and maintenance and fulfills its function by regulation of various target genes, including *Nphs2*, *Mafb*, and *Magi2*. In line with the differential regulation of WT-1 in CYGB-depleted podocytes as well as in *Cygb*^{-/-} mice, we found that these target genes are CYGB dependently regulated in podocytes. Particularly, MAFB, a WT-1 key target gene, has been shown as well to be essential for kidney development (45). Furthermore, its overexpression in podocytes protects against DN, through the regulation of slit diaphragm proteins, antioxidative enzymes, and the Notch

pathway (46). In addition, LMX1B, a transcription factor crucial for proper differentiation of podocyte precursors, was shown to be downregulated in CYGB-deficient podocytes. Overall, our RNA-seq-based transcriptome data in an AB8/13 cell model illustrate that CYGB influences multiple crucial transcription factors in podocyte biology, indicate its potential relevance to podocytopathies, and suggest that CYGB might therefore represent a potential therapeutic target.

Using GWAS, we discovered an SNP in the 3' intergenic region of the *CYGB* gene, potentially associated with increased albuminuria (Fig. 6A). The SNP coincides with a region displaying several hallmarks of an enhancer and loops back to the first intron of *CYGB* gene close to the transcription initiation site as indicated by ChIA-PET data. Consistent with the chromatin looping data, reporter gene assays provide evidence for a cooperation between the distal downstream 3'-enhancer and the proximal *CYGB* promoter in regulating *CYGB* expression. Although additional studies under experimental conditions would be required to validate a potential direct effect of the SNP on *CYGB* gene regulation, these experiments indicate a further correlation of the SNP and the *CYGB* gene locus. Intriguingly, this is the first time that a globin gene was associated with CKD. Simultaneously, the potential role of CYGB in acquired human renal disease was found in an unbiased way by analyzing transcriptomic data of patients with different stages of renal failure (Fig. 6B, C).

In conclusion, our study demonstrates that CYGB (i) is abundantly expressed in human podocyte cell lines, (ii) protects podocytes from oxidative stress and apoptosis, (iii) is required to preserve renal function possibly *via* a podocyte-associated protective role, and (iv) is implicated in CKD.

Materials and Methods

Reagents

AMA (Sigma-Aldrich, St. Louis, MO) was dissolved in 95% ethanol. H₂O₂ was purchased from Sigma-Aldrich. H₂DCFDA (10 μM; Invitrogen, Thermo Fischer Scientific, Waltham, MA) was dissolved in dimethyl sulfoxide (DMSO). 3-(4,5-dimethylthiazol-2-yl)-2,5-diphenyltetrazoliumbromide (MTT; Sigma-Aldrich) for MTT assays was dissolved in phosphate-buffered saline (PBS). For the analysis of human renal biopsies, TaqMan reagents for human *CYGB* (NM_134268) were purchased from Applied Biosystems (Waltham, MA). D-glucose solution and D-mannitol were purchased from Sigma-Aldrich. The OxyBlot protein oxidation kit (S7150) was purchased from Sigma-Aldrich. Hematoxylin and eosin solutions were purchased from Sigma-Aldrich.

Renal function analysis and tissue sampling of *Cygb*-deficient mice

C57BL/6 *Cygb* global knockout mice were generated as described previously (65). To evaluate whether there was a difference in baseline renal function compared with wild-type C57BL/6, glomerular filtration rate (GFR) was determined by measuring FITC-sinistrin clearance. FITC-sinistrin is a fluorescent inulin analog, which is only excreted *via* glomerular filtration (52). For these experiments, nine male *Cygb*^{+/+} and nine male *Cygb*^{-/-} mice (age 18 weeks) were

implanted with two osmotic minipumps (model 1002, release rate of 0.25 μL/h for 14 days; ALZET, Charles River, Beerse, Belgium) filled with 100 mg/mL FITC-sinistrin (Fresenius Kabi Austria GmbH, Linz, Austria), 2 weeks before sacrifice. Mice were anesthetized *via* intraperitoneal injection with a mixture of ketamine (80 mg/kg) and xylazine (16 mg/kg) in 0.9% NaCl and kept on a heating pad (37°C) during surgery. After midline depilation with Veet cream and skin sterilization with ethanol, a ventrolateral incision (0.5 cm) was made and pumps were placed into the peritoneal cavity. The incision was closed with sterile suture, muscle and skin separately. Mice regained consciousness and mobility under partial exposure to a heating lamp, after which they were put into their housing cages. The two-pump strategy was based on the report of Qi *et al.* assuring sufficient serum FITC-sinistrin levels for renal function assessment (54). For final GFR calculation, we applied the equation "FITC-sinistrin clearance = FITC-sinistrin pump infusion rate/steady-state blood FITC-sinistrin concentration" (54).

Twenty-four hours before sacrifice, mice were put in metabolic cages with free access to water and food for 24-h urine collection. Urine was stored at -20°C until further analyses. At sacrifice, mice were deeply anesthetized and exsanguinated *via* the vena cava inferior for blood collection. Serum was extracted and kept at -20°C for further analyses. Kidneys were isolated, decapsulated, weighed, sliced in 1 mm transverse sections, and snap frozen in liquid nitrogen or fixed in neutral buffered formalin. Urine and serum parameters, Na⁺ and K⁺ concentrations, were determined using an electrolyte analyzer (IL-943; Instrumentation Laboratories, Bedford, MA). Osmolality was measured using the Fiske One-Ten osmometer (Fiske, Norwood, MA). Albuminuria was assessed by loading 5 μL of urine sample on a polyacrylamide gel and bovine serum albumin was used as positive control.

All experimental procedures were performed in accordance with the National Institutes of Health Guide for the Care and Use of Laboratory Animals and approved by the University of Antwerp Ethics Committee (permit 2016-47).

Immunohistochemistry

Paraffin-embedded kidney sections were deparaffinized, hydrated, blocked, and incubated overnight with anti-Wt-1 (ab89901; Abcam, Cambridge, United Kingdom). After washing, sections were incubated with a biotinylated goat anti-rabbit immunoglobulin G antibody (Vector Laboratories, Burlingame, CA) and subsequently incubated with avidin and biotinylated horseradish peroxidase (Vector Laboratories). A dark brown color was developed with diaminobenzidine in the presence of 3% H₂O₂. Sections were counterstained with hematoxylin and eosin and mounted in Eukitt (Sigma-Aldrich). Podocyte counts were assessed by staining kidney sections for Wt-1 and quantification was performed in a blinded manner. Glomerular diameters of 30 glomeruli/section were measured from five mice per experimental group using ImageJ. Glomerular volume was determined as $Gv = \beta / k \cdot (\pi \cdot r^2)^{3/2}$, where $\beta = 1.38$ is the shape coefficient for spheres, $k = 1.1$ is the size distribution coefficient, and $(\pi \cdot r^2)$ is the glomerular area (58). For immunofluorescence experiments, *Cygb* staining on *Cygb*^{+/+} and *Cygb*^{-/-} kidneys was performed using anti-*Cygb* (D-7, sc365246; Santa Cruz

Biotechnology, Dallas, TX) and the Vector mouse on mouse immunodetection kit, fluorescein (FMK-2201; Vector Laboratories) according to the manufacturer's instructions. Subsequently, sections were mounted with 4',6-diamidino-2-phenylindole Fluoromount-G (SouthernBiotech, Birmingham, AL) and visualized using fluorescence microscopy.

Cell culture and treatments

Conditionally immortalized human podocyte cell lines AB8/13 and LY were a kind gift from A. Kistler (57). Cells were cultured in Roswell Park Memorial Institute (RPMI) (Sigma-Aldrich) supplemented with 10% heat-inactivated fetal calf serum (FCS; Gibco, Thermo Fischer Scientific), 50 IU/mL penicillin, 50 μ g/mL streptomycin (Invitrogen), 5 μ g/mL insulin, 5 μ g/mL transferrin, and 5 ng/mL sodium selenite (ITS; Roche, Mannheim, Germany). AB8/13 cells were propagated at 33°C and differentiated for 10–14 days at 37°C in a humidified incubator containing 5% CO₂ (Binder, Tuttlingen, Germany). Cell death was measured by the Vi-Cell XR 2.03 Cell Viability Analyzer (Beckman Coulter, Krefeld, Germany) and TC20 automated cell counter (BioRad) using the trypan blue dye exclusion method. HPRT, HEK293T, TK-173, TK-188, and TZ-1 cells were cultured in HG Dulbecco's Modified Eagle Medium (DMEM) (Sigma-Aldrich) supplemented with 10% heat-inactivated FCS, 50 IU/mL penicillin, and 50 μ g/mL streptomycin (Invitrogen). HK-2 were cultured in DMEM/F12 (Sigma-Aldrich) supplemented with 10% heat-inactivated FCS, 100 U/mL penicillin, 100 μ g/mL streptomycin, 36 ng/mL hydrocortisone, 5 μ g/mL insulin, 5 μ g/mL transferrin, and 5 ng/mL selenium (ITS) solution (Roche).

mRNA and protein detection and quantification

Total cellular RNA was extracted as previously described (29). Total RNA (2 μ g) was reverse transcribed (RT) using the Prime Script RT reagent kit (Takara Bio) and cDNA levels were estimated by qPCR using the primers listed in Supplementary Table S5 and a SYBRGreen qPCR reagent kit (Sigma-Aldrich) in a CFX96 C1000 Thermal Cycler (BioRad). Transcript levels were calculated as described before (28) and displayed as fold change, if not otherwise indicated.

Immunoblotting, signal imaging, and quantification were performed as previously reported (47). Membranes were probed with antibodies against CYGB (13317-AP; Proteintech, Rosemont, IL; or EPR13198; Abcam), synaptopodin (SYNPO) (P-19, sc-21537; Santa Cruz Biotechnology), PARP1 ([E102], ab32138; Abcam), cleaved PARP1 ([E51], ab32064; Abcam), TATA-box binding protein (8515; Cell Signaling Technology, Leiden, The Netherlands), β -actin (A5441; Sigma-Aldrich) and α -tubulin (TU-02, sc-8035; Santa Cruz Biotechnology). Signals from horseradish peroxidase (HRP)-coupled secondary antibodies were detected with ECL substrate (Pierce, Thermo Fisher Scientific) using a luminescent image analyzer (Fusion FX6; Vilber Lourmat, Marne la Vallée, France). Uncropped immunoblots are provided in Supplementary Figure S8. Protein oxidation was detected by the OxyBlot method following the manufacturer's instructions. Briefly, each specimen was divided in two aliquots: one aliquot was subjected to derivatization reaction (2,4-dinitrophenylhydrazine solution), while the other one served as a negative control (derivatization-control solution). The treated samples and the corresponding negative control

were loaded into a polyacrylamide gel. After gel electrophoresis, transfer, and blocking, the membrane was incubated with a primary antibody specific to the dinitrophenyl moiety of the proteins, HRP-coupled secondary antibody, and finally exposed on autoradiography film.

Generation of stable knockdown and overexpression cell lines

Expression vectors encoding shRNA sequences targeting human CYGB in a pLKO.1-puro plasmid were purchased from Sigma-Aldrich (shCYGB-1: order number TRCN0000059378; shCYGB-2: order number TRCN0000059381). Control cells (shCTR) were transfected with a nontargeting control shRNA under the control of a U6 promoter in a pLKO.1 puromycin resistance vector (Sigma-Aldrich) as described previously (16). Viral particles were produced in HEK293T cells by cotransfection of the respective transfer vector (3 μ g) with the packaging plasmids pLP1 (4.2 μ g), pLP2 (2 μ g), and pVSV-G (2.8 μ g; all from Invitrogen) using polyethylenimine transfection as described before (15). Cells were transduced with lentiviral-pseudotyped particles, and cell pools were cultured with the appropriate antibiotic for selection. For stable overexpression, full-length human CYGB gene and control gene β -glucuronidase (*GUS*) were cloned into a pLENTI6 plasmid. Viral particles were produced as described above.

H₂DCFDA assay

AB8/13 cells were seeded in 96-well plates at 80% confluency and incubated with 10 μ M H₂DCFDA for 30 min in the dark. Fluorescence was measured using a 96-well fluorometer (Infinite 200Pro; Tecan, Männedorf, Switzerland). Results from kinetic measurements were calculated as described previously (21). Analysis was performed using the internal software i9 control.

roGFP2-Orp1 measurements

AB8/13 cells were grown on glass-bottomed dishes (Ibidi GmbH, Martinsried, Germany) and transduced with the H₂O₂-sensitive probe roGFP2-Orp1 (22, 44), which was subcloned into the pAd/CMV/V5-DEST adenoviral vector (Invitrogen) using the Gateway technology. After 48 h, the oxidation of the sensor was measured at basal level or upon AMA treatment (50 μ g/mL, 30 min). The live measurements of roGFP2 oxidation and calculations of the degree of oxidation were performed as previously described (70).

Cell viability assay

For the MTT assay, AB8/13 cells were seeded in 96-well flat-bottomed plates and then exposed to AMA or H₂O₂ at the indicated concentrations (final volume 0.1 mL per well). After 6 h, 10 μ L of 5 mg/mL MTT solution in PBS was added for 2 h. Following removal of the medium, 100 μ L of DMSO was added to dissolve the formazan crystals. The absorbance at 540 nm was determined in triplicate using a plate reader (Infinite 200Pro; Tecan) and normalized by nontreated cells.

TUNEL assay

Cells were seeded on coverslips and treated with 250 μ M H₂O₂ for 3 h. TUNEL of nuclei was performed using the

APO-BrdU *in situ* DNA fragmentation assay kit (K401-60; Biovision, Milpitas, CA) following the manufacturer's protocol.

Determination of cellular bioenergetics

Differentiated human podocytes were seeded on XF^c24-well microplates (Agilent Technologies, Santa Clara, CA) at 1.5×10^4 cells per well and incubated at 37°C and 5% CO₂ the day before the experiment. The medium was then replaced by RPMI 1640 without bicarbonate, and cells were kept in an incubator without CO₂ before transfer to a Seahorse analyzer XF^c24 (Agilent Technologies), to measure the OCR. Three measurements of OCR were performed at steady state and after sequential injection of 1 μM oligomycin, 2 μM FCCP, and a mix of 0.5 μM rotenone and 0.5 μM AMA. During the experiment, the cells were kept in a humidified chamber at 37°C, under normal oxygen conditions. At the end of the assay, total protein per well was measured using the Bradford reagent (BioRad, Hercules, CA) and OCR values were normalized to the protein amount.

Analysis of human renal biopsies

Human renal biopsy specimens and Affymetrix microarray expression data (HG-U133 Plus2.0 Array; Affymetrix, Santa Clara, CA) were obtained within the framework of the European Renal cDNA Bank–Kröner-Fresenius Biopsy Bank (8). Diagnostic renal biopsies were obtained from patients after informed consent and with approval of the local ethics committees. Following renal biopsy, the tissue was transferred to RNase inhibitor and microdissected into glomerular (Glom) and tubulointerstitial (Tub) compartments. The microarray expression data used in this study came from individual patients with DN (Glom [$n=7$], Tub [$n=7$]), FSGS (Glom [$n=16$], Tub [$n=7$]), rapidly progressive glomerulonephritis (RPGN, Glom [$n=23$], Tub [$n=21$]), minimal change disease (Glom [$n=5$], Tub [$n=5$]), as well as pretransplant biopsies from living renal allograft donors as controls (living donors [LD], Glom [$n=18$], Tub [$n=18$]). Total RNA was isolated from microdissected glomeruli and tubulointerstitium, reverse transcribed, and linearly amplified according to a protocol previously reported (9). Fragmentation, hybridization, staining, and imaging were performed following the Affymetrix expression analysis technical manual (Affymetrix). The raw data were normalized using Robust Multichip Algorithm and annotated by Human Entrez Gene custom CDF annotation version 18. To identify differentially expressed genes, the Significance Analysis of Microarrays method was applied using TiGR (MeV, Version 4.8.1) (71). A q -value below 5% was considered to be statistically significant. RT-qPCR validation of renal biopsies was performed as reported earlier (8, 59). Pre-developed TaqMan reagents were used for human *CYGB* (NM_134268), and transcript levels were normalized to β -actin levels (LD, Glom [$n=9$], Tub [$n=5$], DN, Glom [$n=12$], Tub [$n=15$], FSGS Glom [$n=16$], Tub [$n=17$]), RPGN Glom [$n=9$], Tub [$n=9$]).

Genome-wide association study

Genetic association testing for urinary albumin-to-creatinine ratio, and meta-analysis was performed in the CKDGen and CARE cohorts of European ancestry, with

further follow-up genetic analysis of significant SNPs in CARE cohorts of African American ancestry and in the Diabetes Control and Complications Trial/Epidemiology of Diabetes Interventions and Complications Study, as previously described (3).

RNA-seq library preparation and transcriptome sequencing

Total RNA from three independent samples of shCTR and shCYGB-1 AB8/13 cells was extracted using the RNeasy mini kit according to the manufacturer's instructions (Qiagen, Hilden, Germany). Before library construction, RNA quality was assessed using an Agilent 2100 Bioanalyzer and the Agilent RNA 6000 Nano Kit (Agilent Technologies). RNA integrity number values ranged from 8.5 to 9.7, indicating high-quality RNA samples. RNA was quantified using the Qubit RNA HS Assay Kit (Invitrogen). Libraries were prepared starting from 800 ng of total RNA using the TruSeq Stranded mRNA HT Sample Prep Kit (Illumina), including a poly-A selection step following the manufacturer's instructions and sequenced as 2×150 nt paired-end reads using an Illumina NextSeq 500™. Library preparation and sequencing were performed by StarSEQ® GmbH (Mainz, Germany). RNA-Seq data are available at the European Nucleotide Archive under accession number PRJEB30641.

Differential gene expression, GO term annotation, and pathway enrichment analyses

Raw sequences were preprocessed to remove low-quality reads and residual Illumina adapter sequences using FASTX-Toolkit 0.0.14. The overall sequencing quality and the absence of adapter contamination were evaluated with FastQC 0.11.2. Preprocessed reads were mapped against the annotated human genome version *hg38* with the RNA-seq algorithm of CLC Genomics Workbench 8.5.1 using the following parameters: mismatch cost=2, insertion cost=3, deletion cost=3, length fraction=0.95, and similarity fraction=0.95. The mapping step was performed allowing either one (single) or up to 10 (multiple) mappings for each read, and all the downstream statistical and bioinformatic analyses were computed for both mapping outputs. As the results of the downstream analyses for single or multiple mapping converged (data not shown), only the results obtained with multiple mapping (the library of 2×150 nt paired-end stranded reads minimizes the occurrence of un-specific read mappings) were included. A summary of the mapping statistics is shown in Supplementary Table S6. PCA was performed and visualized using the plotPCA function of DESeq2 (38) (ntop=1000) and ggplot2 (73) R packages (Supplementary Fig. 6C, D). Sample-to-sample distance was calculated from the transformed count matrices and visualized as heatmap using the Pheatmap R package. Both approaches indicated a clear separation among the shCTR- and shCYGB-derived data sets. In particular, PC1 accounted for 87% of the variance.

Differentially expressed genes were determined using the EdgeR-based [Empirical analysis of differential gene expression; (55, 56)] statistical tool of CLC Genomics Workbench using default parameters. Genes were considered differentially expressed when presenting $|\text{fold change}| > 2$ and false discovery rate-corrected p -value ≤ 0.05 . GO term and

KEGG pathway enrichment analyses were performed using WebGestalt (version 2017) using the overrepresentation enrichment analysis method, requiring a Benjamini–Hochberg (BH)-corrected p -value ≤ 0.05 and a minimum enrichment of four genes for term/pathway. Enrichment in canonical pathways and Tox functions were performed with Qiagen's IPA (Qiagen) Core analysis tool using bias-corrected z -score (when applicable) and BH-corrected p -values ≤ 0.05 .

Luciferase reporter gene assays

A 90 bp oligonucleotide encompassing the rs8082416 SNP was cloned into pGL3prom (Promega) between the *MluI* and *XhoI* restriction sites. The CYGB promoter was amplified by PCR from genomic DNA of HEK293T cells and cloned into pGL3basic (Promega). If not otherwise indicated, 3×10^5 HEK293T cells were transiently transfected with 500 ng reporter plasmid in a six-well format using Roti-Fect (Carl Roth, Karlsruhe, Germany). To control for differences in transfection efficiency and extract preparation, 5 ng pRL-SV40 *Renilla* luciferase reporter vector (Promega) was co-transfected. Cultures were evenly split onto 24-well plates 24 h after transfection. Luciferase activities of triplicate wells were determined using the dual-luciferase reporter assay system (Promega) as described before (62). Reporter activities were expressed as relative firefly/*Renilla* luciferase activities. All reporter gene assays were performed at least three times independently.

Statistical analyses

If not otherwise indicated, results are presented as mean values \pm standard errors of the mean of at least three independent experiments. Statistical analyses were performed using Student's t -test and one-way analysis of variance (ANOVA) or two-way ANOVA, where appropriate. p -Values < 0.05 were considered statistically significant. For the human biopsy data, statistical analysis was performed using Kruskal–Wallis and Mann–Whitney tests (SPSS 24.0; SPSS, Inc., Chicago, IL).

Acknowledgments

We thank Gerhard Müller and Michael Zeisberg for providing TK173, TK188, and TZ-1 cells, Moin Saleem for providing two podocyte cell lines, Caroline Fox, Ming-Huei Chen, and the CKDGen Consortium for interrogating urinary albumin-to-creatinine ratio data sets, Patrick D'Haese and Jean-Pierre Montani for advice, Julia Birk and Marcel Saarbeck for cloning assistance, Joey De Backer as well as all Hoogewijs laboratory members for advice and technical support. We also thank the participating centers of the European Renal cDNA Bank–Kröner-Fresenius biopsy bank (ERCB-KFB) and their patients for their cooperation.

Author Disclosure Statement

No competing financial interests exist.

Funding Information

This work was supported by the Swiss National Science Foundation (grant 173000) and the German Research Foun-

ation (grant HO5837/1-1) to D.H., a University Research Priority Program “Integrative Human Physiology” grant to E.B.R., the Biobank ERCB-KFB (Else Kröner-Fresenius-Foundation) to C.D.C., an intramural grant (Center for Computer Sciences, JGU Mainz) to T.H., the International PhD Program (IMB Mainz) to E.P. and T.H., a Grant-in-Aid for Scientific Research from JSPS (No. 25293177 and No. 16H05290) and a Grant for Research Program on Hepatitis from the Japan Agency for Medical Research and Development (18fk0210004h0003) to N.K., and the NCCR Kidney.CH financed by the SNF to C.D.C., O.D., A.O., R.H.W., and D.H.

Supplementary Material

Supplementary Figure S1
 Supplementary Figure S2
 Supplementary Figure S3
 Supplementary Figure S4
 Supplementary Figure S5
 Supplementary Figure S6
 Supplementary Figure S7
 Supplementary Figure S8
 Supplementary Table S1
 Supplementary Table S2
 Supplementary Table S3
 Supplementary Table S4
 Supplementary Table S5
 Supplementary Table S6

References

- Balkawade RS, Chen C, Crowley MR, Crossman DK, Clapp WL, Verlander JW, and Marshall CB. Podocyte-specific expression of Cre recombinase promotes glomerular basement membrane thickening. *Am J Physiol Renal Physiol* 316: F1026–F1040, 2019.
- Betz B and Conway BR. An update on the use of animal models in diabetic nephropathy research. *Curr Diab Rep* 16: 18, 2016.
- Böger CA, Chen MH, Tin A, Olden M, Kottgen A, de Boer IH, Fuchsberger C, O'Seaghdha CM, Pattaro C, Teumer A, Liu CT, Glazer NL, Li M, O'Connell JR, Tanaka T, Peralta CA, Kutalik Z, Luan J, Zhao JH, Hwang SJ, Akyzbekova E, Kramer H, van der Harst P, Smith AV, Lohman K, de Andrade M, Hayward C, Kollerits B, Tonjes A, Aspelund T, Ingelsson E, Eiriksdottir G, Launer LJ, Harris TB, Shuldiner AR, Mitchell BD, Arking DE, Franceschini N, Boerwinkle E, Egan J, Hernandez D, Reilly M, Townsend RR, Lumley T, Siscovick DS, Psaty BM, Kestenbaum B, Haritunians T, Bergmann S, Vollenweider P, Waeber G, Mooser V, Waterworth D, Johnson AD, Florez JC, Meigs JB, Lu X, Turner ST, Atkinson EJ, Leak TS, Aasarod K, Skorpen F, Syvanen AC, Illig T, Baumert J, Koenig W, Kramer BK, Devuyst O, Mychaleckyj JC, Minelli C, Bakker SJ, Kedenko L, Paulweber B, Coassin S, Endlich K, Kroemer HK, Biffar R, Stracke S, Volzke H, Stumvoll M, Magi R, Campbell H, Vitart V, Hastie ND, Gudnason V, Kardina SL, Liu Y, Polasek O, Curhan G, Kronenberg F, Prokopenko I, Rudan I, Arnlöv J, Hallan S, Navis G, Parsa A, Ferrucci L, Coresh J, Shlipak MG, Bull SB, Paterson NJ, Wichmann HE, Wareham NJ, Loos RJ, Rotter JI, Pramstaller PP, Cupples LA, Beckmann JS, Yang Q, Heid IM, Rettig R, Dreisbach AW, Bochud M, Fox CS, and Kao

- WH. CUBN is a gene locus for albuminuria. *J Am Soc Nephrol* 22: 555–570, 2011.
4. Bryniarski MA, Yee BM, Jaffri I, Chaves LD, Yu JA, Guan X, Ghavam N, Yacoub R, and Morris ME. Increased megalin expression in early type 2 diabetes: role of insulin signaling pathways. *Am J Physiol Renal Physiol* 315: F1191–F1207, 2018.
 5. Burmester T, Ebner B, Weich B, and Hankeln T. Cyto-globin: a novel globin type ubiquitously expressed in vertebrate tissues. *Mol Biol Evol* 19: 416–421, 2002.
 6. Burmester T and Hankeln T. Function and evolution of vertebrate globins. *Acta Physiol (Oxf)* 211: 501–514, 2014.
 7. Burmester T, Weich B, Reinhardt S, and Hankeln T. A vertebrate globin expressed in the brain. *Nature* 407: 520–523, 2000.
 8. Cohen CD, Frach K, Schlondorff D, and Kretzler M. Quantitative gene expression analysis in renal biopsies: a novel protocol for a high-throughput multicenter application. *Kidney Int* 61: 133–140, 2002.
 9. Cohen CD, Klingenhoff A, Boucherot A, Nitsche A, Henger A, Brunner B, Schmid H, Merkle M, Saleem MA, Koller KP, Werner T, Grone HJ, Nelson PJ, and Kretzler M. Comparative promoter analysis allows de novo identification of specialized cell junction-associated proteins. *Proc Natl Acad Sci U S A* 103: 5682–5687, 2006.
 10. Davis CA, Hitz BC, Sloan CA, Chan ET, Davidson JM, Gabdank I, Hilton JA, Jain K, Baymuradov UK, Narayanan AK, Onate KC, Graham K, Miyasato SR, Dreszer TR, Strattan JS, Jolanki O, Tanaka FY, and Cherry JM. The encyclopedia of DNA elements (ENCODE): data portal update. *Nucleic Acids Res* 46: D794–D801, 2018.
 11. Dong L, Pietsch S, Tan Z, Perner B, Sierig R, Kruspe D, Groth M, Witzgall R, Grone HJ, Platzer M, and Englert C. Integration of cistromic and transcriptomic analyses identifies Nphs2, Mafb, and Magi2 as Wilms' tumor 1 target genes in podocyte differentiation and maintenance. *J Am Soc Nephrol* 26: 2118–2128, 2015.
 12. Fordel E, Thijs L, Martinet W, Lenjou M, Laufs T, Van Bockstaele D, Moens L, and Dewilde S. Neuroglobin and cytoglobin overexpression protects human SH-SY5Y neuroblastoma cells against oxidative stress-induced cell death. *Neurosci Lett* 410: 146–151, 2006.
 13. Fordel E, Thijs L, Martinet W, Schrijvers D, Moens L, and Dewilde S. Anoxia or oxygen and glucose deprivation in SH-SY5Y cells: a step closer to the unraveling of neuroglobin and cytoglobin functions. *Gene* 398: 114–122, 2007.
 14. Fordel E, Thijs L, Moens L, and Dewilde S. Neuroglobin and cytoglobin expression in mice. Evidence for a correlation with reactive oxygen species scavenging. *FEBS J* 274: 1312–1317, 2007.
 15. Fuady JH, Bordoli MR, Abreu-Rodriguez I, Kristiansen G, Hoogewijs D, Stiehl DP, and Wenger RH. Hypoxia-inducible factor-mediated induction of WISP-2 contributes to attenuated progression of breast cancer. *Hypoxia (Auckl)* 2: 23–33, 2014.
 16. Fuady JH, Gutsche K, Santambrogio S, Varga Z, Hoogewijs D, and Wenger RH. Estrogen-dependent downregulation of hypoxia-inducible factor (HIF)-2alpha in invasive breast cancer cells. *Oncotarget* 7: 31153–31165, 2016.
 17. Gardner AM, Cook MR, and Gardner PR. Nitric-oxide dioxygenase function of human cytoglobin with cellular reductants and in rat hepatocytes. *J Biol Chem* 285: 23850–23857, 2010.
 18. Geuens E, Brouns I, Flamez D, Dewilde S, Timmermans JP, and Moens L. A globin in the nucleus! *J Biol Chem* 278: 30417–30420, 2003.
 19. Gnudi L. Cellular and molecular mechanisms of diabetic glomerulopathy. *Nephrol Dial Transplant* 27: 2642–2649, 2012.
 20. Guo JK, Menke AL, Gubler MC, Clarke AR, Harrison D, Hammes A, Hastie ND, and Schedl A. WT1 is a key regulator of podocyte function: reduced expression levels cause crescentic glomerulonephritis and mesangial sclerosis. *Hum Mol Genet* 11: 651–659, 2002.
 21. Gutsche K, Randi EB, Blank V, Fink D, Wenger RH, Leo C, and Scholz CC. Intermittent hypoxia confers prometastatic gene expression selectively through NF-kappaB in inflammatory breast cancer cells. *Free Radic Biol Med* 101: 129–142, 2016.
 22. Gutsche M, Sobotta MC, Wabnitz GH, Ballikaya S, Meyer AJ, Samstag Y, and Dick TP. Proximity-based protein thiol oxidation by H₂O₂-scavenging peroxidases. *J Biol Chem* 284: 31532–31540, 2009.
 23. Ha H, Hwang IA, Park JH, and Lee HB. Role of reactive oxygen species in the pathogenesis of diabetic nephropathy. *Diabetes Res Clin Pract* 82 Suppl 1: S42–S45, 2008.
 24. Halligan KE, Jourd'heuil FL, and Jourd'heuil D. Cytoglobin is expressed in the vasculature and regulates cell respiration and proliferation via nitric oxide dioxygenation. *J Biol Chem* 284: 8539–8547, 2009.
 25. Hankeln T, Ebner B, Fuchs C, Gerlach F, Haberkamp M, Laufs TL, Roesner A, Schmidt M, Weich B, Wystub S, Saaler-Reinhardt S, Reuss S, Bolognesi M, De Sanctis D, Marden MC, Kiger L, Moens L, Dewilde S, Nevo E, Avivi A, Weber RE, Fago A, and Burmester T. Neuroglobin and cytoglobin in search of their role in the vertebrate globin family. *J Inorg Biochem* 99: 110–119, 2005.
 26. Hodges NJ, Innocent N, Dhanda S, and Graham M. Cellular protection from oxidative DNA damage by over-expression of the novel globin cytoglobin in vitro. *Mutagenesis* 23: 293–298, 2008.
 27. Hoogewijs D, Ebner B, Germani F, Hoffmann FG, Fabrizio A, Moens L, Burmester T, Dewilde S, Storz JF, Vinogradov SN, and Hankeln T. Androglobin: a chimeric globin in metazoans that is preferentially expressed in mammalian testes. *Mol Biol Evol* 29: 1105–1114, 2012.
 28. Hoogewijs D, Houthoofd K, Matthijssens F, Vandesompele J, and Vanfleteren JR. Selection and validation of a set of reliable reference genes for quantitative SOD gene expression analysis in *C. elegans*. *BMC Mol Biol* 9: 9, 2008.
 29. Hoogewijs D, Vogler M, Zwenger E, Krull S, and Zieseniss A. Oxygen-dependent regulation of aquaporin-3 expression. *Hypoxia (Auckl)* 4: 91–97, 2016.
 30. Jefferson JA, Shankland SJ, and Pichler RH. Proteinuria in diabetic kidney disease: a mechanistic viewpoint. *Kidney Int* 74: 22–36, 2008.
 31. Latina A, Viticchiè G, Lena AM, Piro MC, Annicchiarico-Petruzzelli M, Melino G, and Candi E. ΔNp63 targets cytoglobin to inhibit oxidative stress-induced apoptosis in keratinocytes and lung cancer. *Oncogene* 35: 1493–1503, 2015.
 32. Lee JW, Chou CL, and Knepper MA. Deep sequencing in microdissected renal tubules identifies nephron segment-specific transcriptomes. *J Am Soc Nephrol* 26: 2669–2677, 2015.
 33. Li D, Chen XQ, Li WJ, Yang YH, Wang JZ, and Yu AC. Cytoglobin up-regulated by hydrogen peroxide plays a

- protective role in oxidative stress. *Neurochem Res* 32: 1375–1380, 2007.
34. Ling Q, Shi W, Huang C, Zheng J, Cheng Q, Yu K, Chen S, Zhang H, Li N, and Chen M. Epigenetic silencing of dual oxidase 1 by promoter hypermethylation in human hepatocellular carcinoma. *Am J Cancer Res* 4: 508–517, 2014.
 35. Liu BC, Song X, Lu XY, Li DT, Eaton DC, Shen BZ, Li XQ, and Ma HP. High glucose induces podocyte apoptosis by stimulating TRPC6 via elevation of reactive oxygen species. *Biochim Biophys Acta* 1833: 1434–1442, 2013.
 36. Liu X, El-Mahdy MA, Boslett J, Varadharaj S, Hemann C, Abdelghany TM, Ismail RS, Little SC, Zhou D, Thuy LT, Kawada N, and Zweier JL. Cytoglobin regulates blood pressure and vascular tone through nitric oxide metabolism in the vascular wall. *Nat Commun* 8: 14807, 2017.
 37. Liu X, Follmer D, Zweier JR, Huang X, Hemann C, Liu K, Druhan LJ, and Zweier JL. Characterization of the function of cytoglobin as an oxygen-dependent regulator of nitric oxide concentration. *Biochemistry* 51: 5072–5082, 2012.
 38. Love MI, Huber W, and Anders S. Moderated estimation of fold change and dispersion for RNA-seq data with DESeq2. *Genome Biol* 15: 550, 2014.
 39. Lu Y, Ye Y, Bao W, Yang Q, Wang J, Liu Z, and Shi S. Genome-wide identification of genes essential for podocyte cytoskeletons based on single-cell RNA sequencing. *Kidney Int* 92: 1119–1129, 2017.
 40. Luxen S, Belinsky SA, and Knaus UG. Silencing of DUOX NADPH oxidases by promoter hypermethylation in lung cancer. *Cancer Res* 68: 1037–1045, 2008.
 41. MacIsaac RJ, Tsalamandris C, Panagiotopoulos S, Smith TJ, McNeil KJ, and Jerums G. Nonalbuminuric renal insufficiency in type 2 diabetes. *Diabetes Care* 27: 195–200, 2004.
 42. Mimura I, Nangaku M, Nishi H, Inagi R, Tanaka T, and Fujita T. Cytoglobin, a novel globin, plays an antifibrotic role in the kidney. *Am J Physiol Renal Physiol* 299: F1120–F1133, 2010.
 43. Miner JH. Podocyte biology in 2015: new insights into the mechanisms of podocyte health. *Nat Rev Nephrol* 12: 63–64, 2016.
 44. Morgan B, Sobotta MC, and Dick TP. Measuring E(GSH) and H₂O₂ with roGFP2-based redox probes. *Free Radic Biol Med* 51: 1943–1951, 2011.
 45. Moriguchi T, Hamada M, Morito N, Terunuma T, Hasegawa K, Zhang C, Yokomizo T, Esaki R, Kuroda E, Yoh K, Kudo T, Nagata M, Greaves DR, Engel JD, Yamamoto M, and Takahashi S. MafB is essential for renal development and F4/80 expression in macrophages. *Mol Cell Biol* 26: 5715–5727, 2006.
 46. Morito N, Yoh K, Ojima M, Okamura M, Nakamura M, Hamada M, Shimohata H, Moriguchi T, Yamagata K, and Takahashi S. Overexpression of MafB in podocytes protects against diabetic nephropathy. *J Am Soc Nephrol* 25: 2546–2557, 2014.
 47. Müller-Edenborn K, Leger K, Glaus Garzon JF, Oertli C, Mirsaidi A, Richards PJ, Rehrauer H, Spielmann P, Hoogewijs D, Borsig L, Hottiger MO, and Wenger RH. Hypoxia attenuates the proinflammatory response in colon cancer cells by regulating IkappaB. *Oncotarget* 6: 20288–20301, 2015.
 48. Nakatani K, Okuyama H, Shimahara Y, Saeki S, Kim DH, Nakajima Y, Seki S, Kawada N, and Yoshizato K. Cytoglobin/STAP, its unique localization in splanchnic fibroblast-like cells and function in organ fibrogenesis. *Lab Invest* 84: 91–101, 2004.
 49. Nishi H, Inagi R, Kawada N, Yoshizato K, Mimura I, Fujita T, and Nangaku M. Cytoglobin, a novel member of the globin family, protects kidney fibroblasts against oxidative stress under ischemic conditions. *Am J Pathol* 178: 128–139, 2011.
 50. O'Seaghdha CM and Fox CS. Genome-wide association studies of chronic kidney disease: what have we learned? *Nat Rev Nephrol* 8: 89–99, 2011.
 51. Petersen MG, Dewilde S, and Fago A. Reactions of ferrous neuroglobin and cytoglobin with nitrite under anaerobic conditions. *J Inorg Biochem* 102: 1777–1782, 2008.
 52. Pill J, Kraenzlin B, Jander J, Sattelkau T, Sadick M, Kloetzer HM, Deus C, Kraemer U, and Gretz N. Fluorescein-labeled sinistrin as marker of glomerular filtration rate. *Eur J Med Chem* 40: 1056–1061, 2005.
 53. Qi Z, Fujita H, Jin J, Davis LS, Wang Y, Fogo AB, and Breyer MD. Characterization of susceptibility of inbred mouse strains to diabetic nephropathy. *Diabetes* 54: 2628–2637, 2005.
 54. Qi ZH, Whitt I, Mehta A, Jin JP, Zhao M, Harris RC, Fogo AB, and Breyer MD. Serial determination of glomerular filtration rate in conscious mice using FITC-inulin clearance. *Am J Physiol Renal Physiol* 286: F590–F596, 2004.
 55. Robinson MD, McCarthy DJ, and Smyth GK. edgeR: a Bioconductor package for differential expression analysis of digital gene expression data. *Bioinformatics* 26: 139–140, 2010.
 56. Robinson MD and Smyth GK. Small-sample estimation of negative binomial dispersion, with applications to SAGE data. *Biostatistics* 9: 321–332, 2008.
 57. Saleem MA, O'Hare MJ, Reiser J, Coward RJ, Inward CD, Farren T, Xing CY, Ni L, Mathieson PW, and Mundel P. A conditionally immortalized human podocyte cell line demonstrating nephrin and podocin expression. *J Am Soc Nephrol* 13: 630–638, 2002.
 58. Samuel T, Hoy WE, Douglas-Denton R, Hughson MD, and Bertram JF. Applicability of the glomerular size distribution coefficient in assessing human glomerular volume: the Weibel and Gomez method revisited. *J Anat* 210: 578–582, 2007.
 59. Schörg A, Santambrogio S, Platt JL, Schödel J, Lindenmeyer MT, Cohen CD, Schrödter K, Mole DR, Wenger RH, and Hoogewijs D. Destruction of a distal hypoxia response element abolishes trans-activation of the PAG1 gene mediated by HIF-independent chromatin looping. *Nucleic Acids Res* 43: 5810–5823, 2015.
 60. Singh S, Canseco DC, Manda SM, Shelton JM, Chirumamilla RR, Goetsch SC, Ye Q, Gerard RD, Schneider JW, Richardson JA, Rothermel BA, and Mammen PP. Cytoglobin modulates myogenic progenitor cell viability and muscle regeneration. *Proc Natl Acad Sci U S A* 111: E129–E138, 2014.
 61. Stagner JI, Seelan RS, Parthasarathy RN, and White K. Reduction of ischemic cell death in cultured Islets of Langerhans by the induction of cytoglobin. *Islets* 1: 50–54, 2009.
 62. Storti F, Santambrogio S, Crowther LM, Otto T, Abreu-Rodríguez I, Kaufmann M, Hu CJ, Dame C, Fandrey J, Wenger RH, and Hoogewijs D. A novel distal upstream hypoxia response element regulating oxygen-dependent erythropoietin gene expression. *Haematologica* 99: e45–e48, 2014.

63. Susztak K, Raff AC, Schiffer M, and Bottinger EP. Glucose-induced reactive oxygen species cause apoptosis of podocytes and podocyte depletion at the onset of diabetic nephropathy. *Diabetes* 55: 225–233, 2006.
64. Thuy LT, Matsumoto Y, Van Thuy TT, Hai H, Suoh M, Urahara Y, Motoyama H, Fujii H, Tamori A, Kubo S, Takemura S, Morita T, Yoshizato K, and Kawada N. Cytoglobin deficiency promotes liver cancer development from hepatosteatosis through activation of the oxidative stress pathway. *Am J Pathol* 185: 1045–1060, 2015.
65. Thuy le TT, Morita T, Yoshida K, Wakasa K, Iizuka M, Ogawa T, Mori M, Sekiya Y, Momen S, Motoyama H, Ikeda K, Yoshizato K, and Kawada N. Promotion of liver and lung tumorigenesis in DEN-treated cytoglobin-deficient mice. *Am J Pathol* 179: 1050–1060, 2011.
66. Thuy le TT, Van Thuy TT, Matsumoto Y, Hai H, Ikura Y, Yoshizato K, and Kawada N. Absence of cytoglobin promotes multiple organ abnormalities in aged mice. *Sci Rep* 6: 24990, 2016.
67. Tian SF, Yang HH, Xiao DP, Huang YJ, He GY, Ma HR, Xia F, and Shi XC. Mechanisms of neuroprotection from hypoxia-ischemia (HI) brain injury by up-regulation of cytoglobin (CYGB) in a neonatal rat model. *J Biol Chem* 288: 15988–16003, 2013.
68. Trandafir F, Hoogewijs D, Altieri F, Rivetti di Val Cervo P, Ramser K, Van Doorslaer S, Vanfleteren JR, Moens L, and Dewilde S. Neuroglobin and cytoglobin as potential enzyme or substrate. *Gene* 398: 103–113, 2007.
69. Trent JT, 3rd, and Hargrove MS. A ubiquitously expressed human hexacoordinate hemoglobin. *J Biol Chem* 277: 19538–19545, 2002.
70. Tsachaki M, Birk J, Egert A, and Odermatt A. Determination of the topology of endoplasmic reticulum membrane proteins using redox-sensitive green-fluorescence protein fusions. *Biochim Biophys Acta* 1853: 1672–1682, 2015.
71. Tusher VG, Tibshirani R, and Chu G. Significance analysis of microarrays applied to the ionizing radiation response. *Proc Natl Acad Sci U S A* 98: 5116–5121, 2001.
72. Vinogradov SN and Moens L. Diversity of globin function: enzymatic, transport, storage, and sensing. *J Biol Chem* 283: 8773–8777, 2008.
73. Wickham H. *ggplot2: Elegant Graphics for Data Analysis*. New York: Springer-Verlag, 2016.
74. Xu R, Harrison PM, Chen M, Li L, Tsui TY, Fung PC, Cheung PT, Wang G, Li H, Diao Y, Krissansen GW, Xu S, and Farzaneh F. Cytoglobin overexpression protects against damage-induced fibrosis. *Mol Ther* 13: 1093–1100, 2006.
75. Yassin M, Kissow H, Vainer B, Joseph PD, Hay-Schmidt A, Olsen J, and Pedersen AE. Cytoglobin affects tumorigenesis and the expression of ulcerative colitis-associated genes under chemically induced colitis in mice. *Sci Rep* 8: 6905, 2018.

Date of first submission to ARS Central, September 6, 2019; date of final revised submission, November 28, 2019; date of acceptance, December 18, 2019.

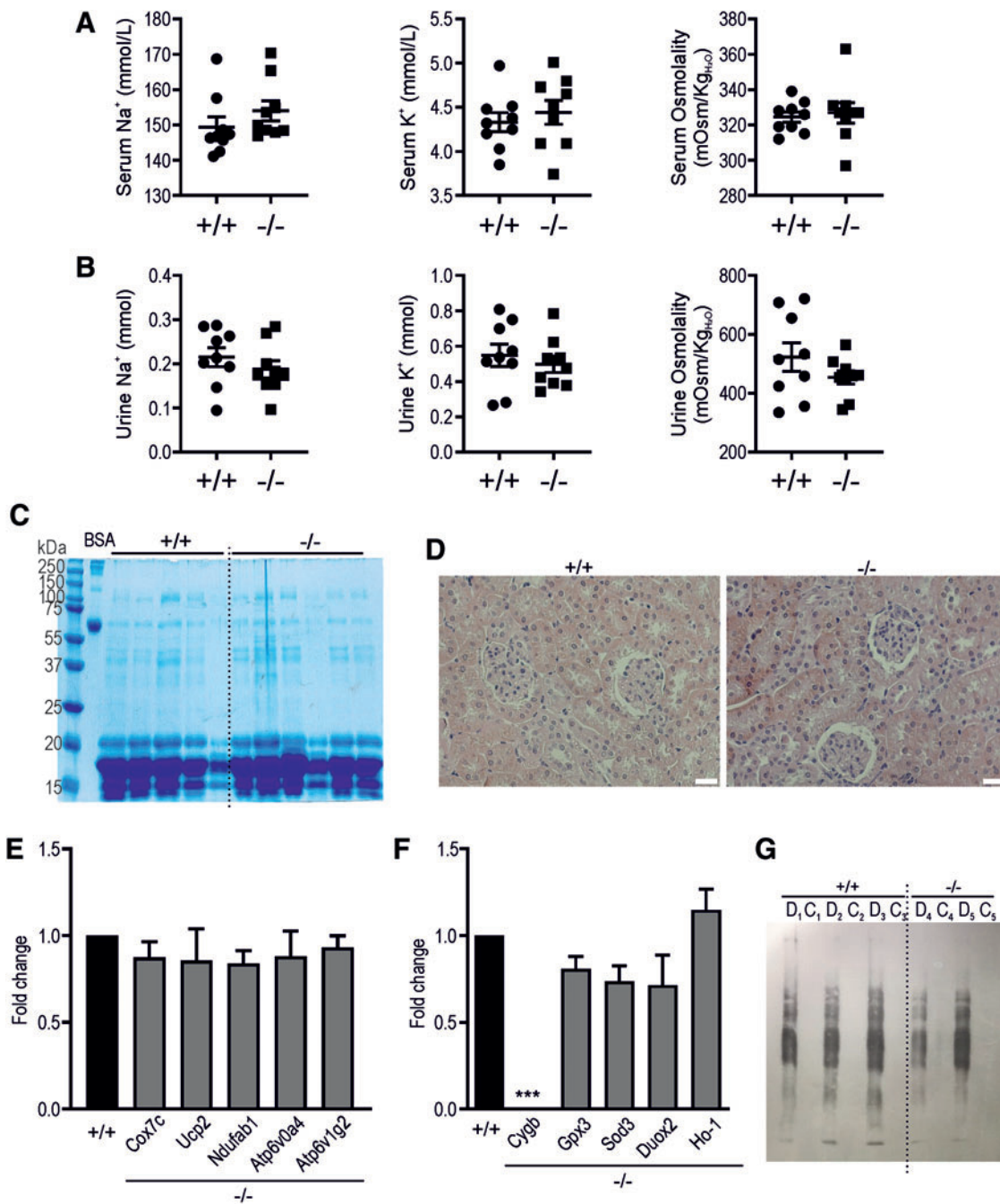
Abbreviations Used

Adgb	= androglobin
AMA	= antimycin A
ANOVA	= analysis of variance
BH	= Benjamini–Hochberg
BSA	= bovine serum albumin
cDNA	= complementary DNA
ChIA-PET	= chromatin interaction analysis by paired-end tag
CKD	= chronic kidney disease
CYGB/Cygb	= human/mouse cytoglobin
DAPI	= 4',6-diamidino-2-phenylindole
DCF	= 2',7'-dichlorofluorescein
DMEM	= Dulbecco's Modified Eagle Medium
DMSO	= dimethyl sulfoxide
DN	= diabetic nephropathy
FCCP	= carbonyl cyanide-4 trifluoromethoxy phenylhydrazone
FCS	= fetal calf serum
FDR	= false discovery rate
FITC	= fluorescein isothiocyanate
FSGS	= focal segmental glomerulosclerosis
GFR	= glomerular filtration rate
Glom	= glomerular
GUS	= β -glucuronidase
GWAS	= genome-wide association studies
H ₂ DCFDA	= 2',7'-dichlorodihydrofluorescein diacetate
Hb	= hemoglobin
HG	= high glucose
HO-1	= heme oxygenase 1
HRP	= horseradish peroxidase
IPA	= ingenuity pathway analysis
LD	= living donors
Mb	= myoglobin
MCD	= minimal change disease
MTT	= 3-(4,5-dimethylthiazol-2-yl)-2,5-diphenyltetrazoliumbromide
Ngb	= neuroglobin
OCR	= oxygen consumption rate
PBS	= phosphate-buffered saline
PCA	= principal component analysis
PI	= propidium iodide
Rot	= rotenone
ROS	= reactive oxygen species
RPGN	= rapidly progressive glomerulonephritis
RPKM	= reads per kilobase per million mapped reads
RPMI	= Roswell Park Memorial Institute
RT-qPCR	= reverse transcription-quantitative polymerase chain reaction
scRNA-seq	= single-cell RNA sequencing
SEM	= standard error of mean
shRNA	= short hairpin RNA
SNP	= single-nucleotide polymorphism
TBP	= TATA-box binding protein
Tub	= tubulointerstitial
TUNEL	= terminal deoxynucleotidyl transferase dUTP nick end labeling

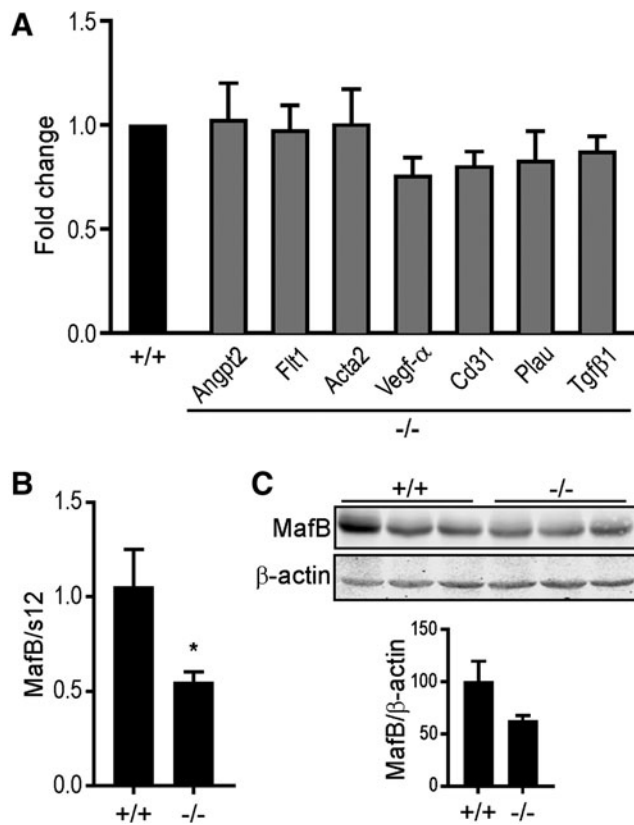
Address correspondence to:
 Prof. David Hoogewijs
 Department of Medicine/Physiology
 University of Fribourg
 Fribourg 1700
 Switzerland

E-mail: david.hoogewijs@unifr.ch

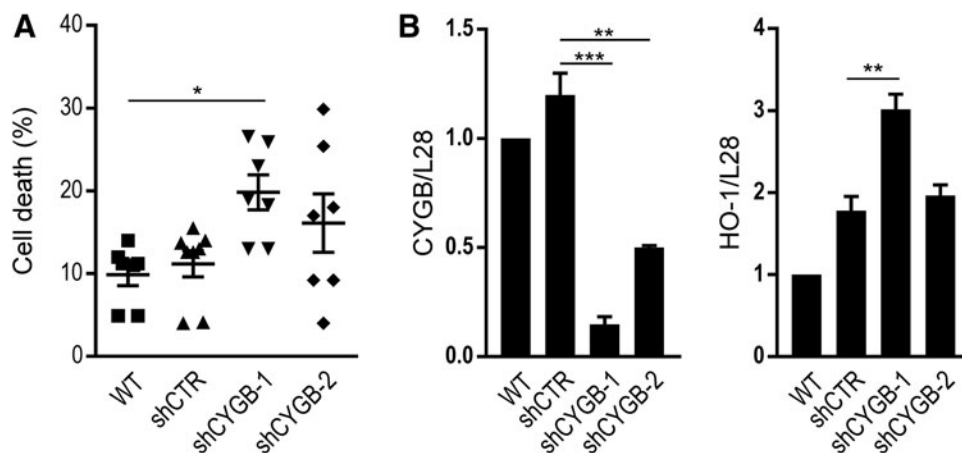
Supplementary Data



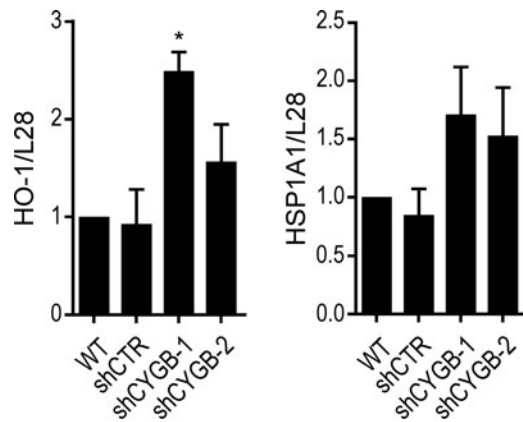
SUPPLEMENTARY FIG. S1. Effect of *Cygb* deficiency on serum and urine parameters. Na⁺, K⁺, and osmolality were assessed for *Cygb*^{+/+} and *Cygb*^{-/-} mice in (A) serum and (B) urine samples. None of the analyzed parameters resulted in significant differences between the two groups. +/+, n=9; -/- n=9. (C) Potential albuminuria assessment on *Cygb*^{+/+} and *Cygb*^{-/-} urine samples. BSA was used as positive control. (D) Hematoxylin and eosin staining of *Cygb*^{+/+} and *Cygb*^{-/-} kidneys. (E) RT-qPCR quantification of metabolism-related genes in whole-kidney lysates of *Cygb*^{+/+} and *Cygb*^{-/-} mice. (F) RT-qPCR quantification of *Cygb* and antioxidative genes in *Cygb*^{+/+} and *Cygb*^{-/-} mice. ****p* < 0.001; one-way ANOVA and Tukey's *post hoc* test. (G) OxyBlot on *Cygb*^{+/+} and *Cygb*^{-/-} mice. Derivatization treated (D) and negative control (C) from the same specimen are displayed with the same number. *Cygb*^{+/+}, n=3; *Cygb*^{-/-} n=2. ANOVA, analysis of variance; BSA, bovine serum albumin; CYGB/*Cygb*, human/mouse cytoglobin; RT-qPCR, reverse transcription-quantitative polymerase chain reaction.



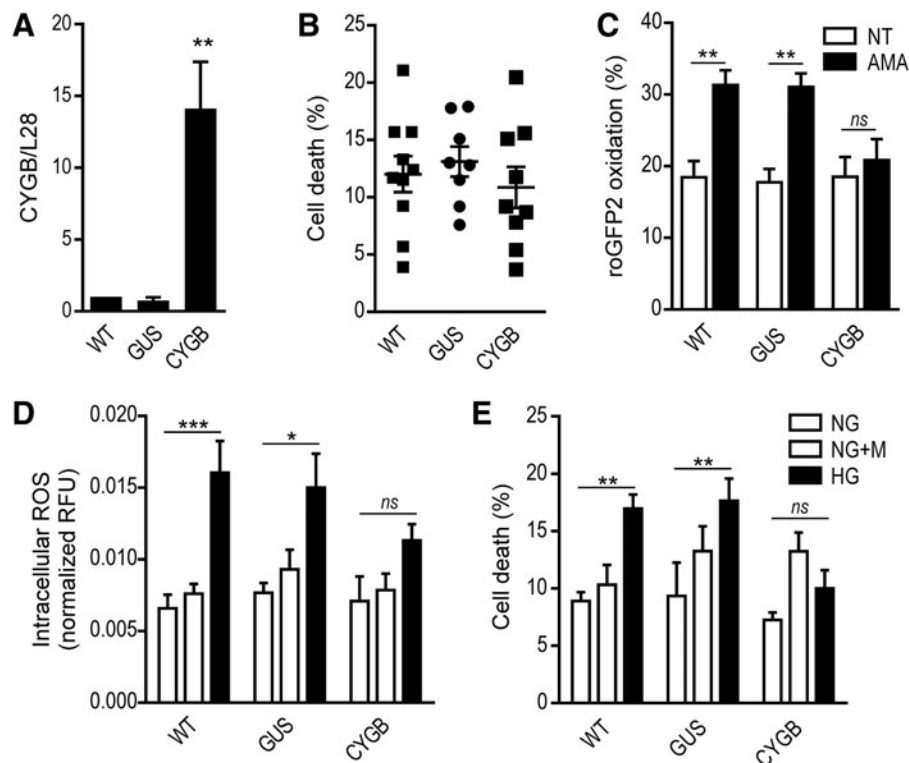
SUPPLEMENTARY FIG. S2. Marker gene and MafB expression in mice. (A) RT-qPCR quantification of fibrosis and vasculature marker genes in *Cygb*^{+/+} and *Cygb*^{-/-} mice. (B) mRNA and (C) protein levels of MafB in *Cygb*^{+/+} and *Cygb*^{-/-} mice and corresponding immunoblot quantification. β -Actin was used as loading control. * $p < 0.05$; Student's *t*-test. Acta2, α -smooth muscle actin; Angpt2, angiopoietin-2; Cd31, cluster of differentiation 31 (also known as Pecam, platelet endothelial cell adhesion molecule); Flt1, vascular endothelial growth factor receptor 1; Plau, plasminogen activator urokinase; Tgf β 1, transforming growth factor beta 1; Vegf- α , vascular endothelial growth factor A.



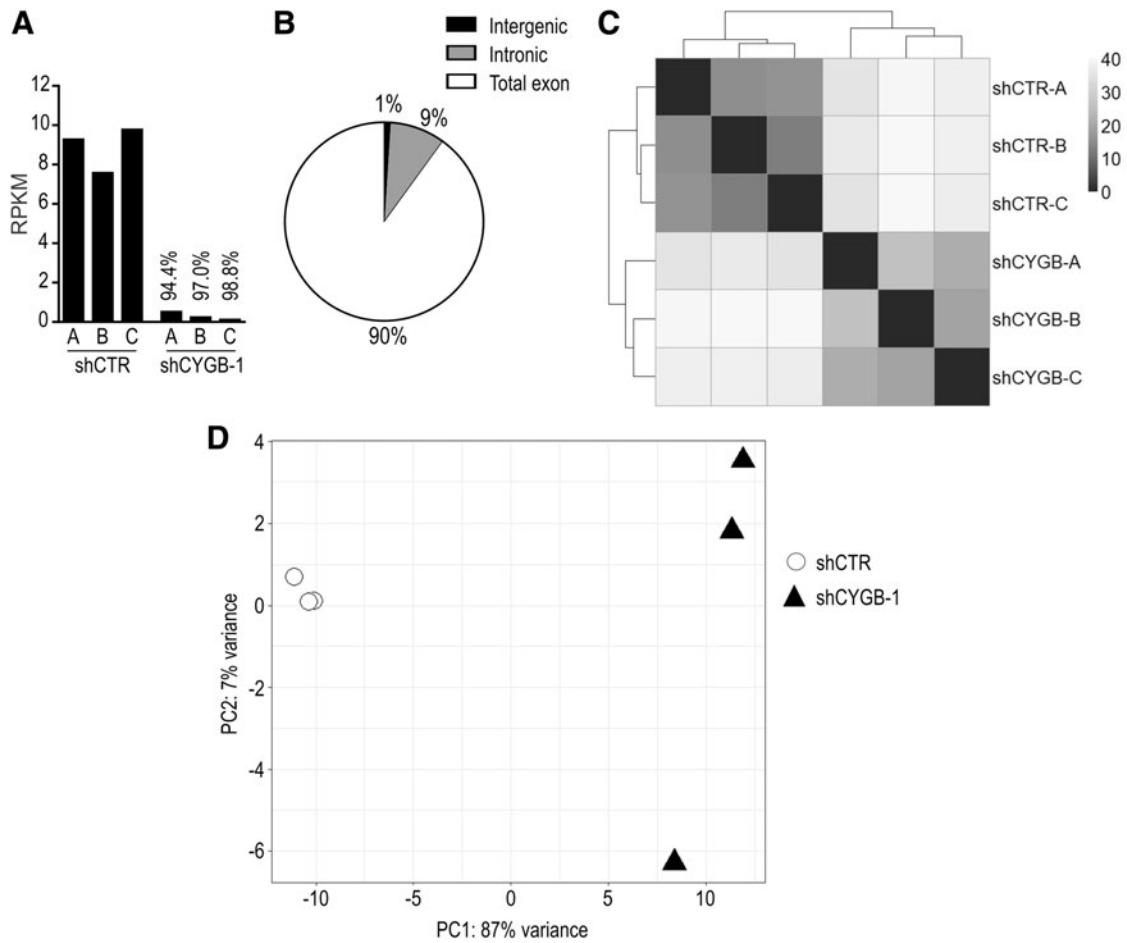
SUPPLEMENTARY FIG. S3. CYGB knockdown in the podocyte cell line LY. (A) Cell death was measured by trypan blue exclusion ($n = 6-8$). * $p < 0.05$; one-way ANOVA and Tukey correction for multiple comparisons. (B) RT-qPCR quantification of CYGB and HO-1 in WT, shCTR, shCYGB-1, and shCYGB-2 cells ($n = 4$). ** $p < 0.01$; *** $p < 0.001$; one-way ANOVA and Tukey's *post hoc* test. HO-1, heme oxygenase 1.



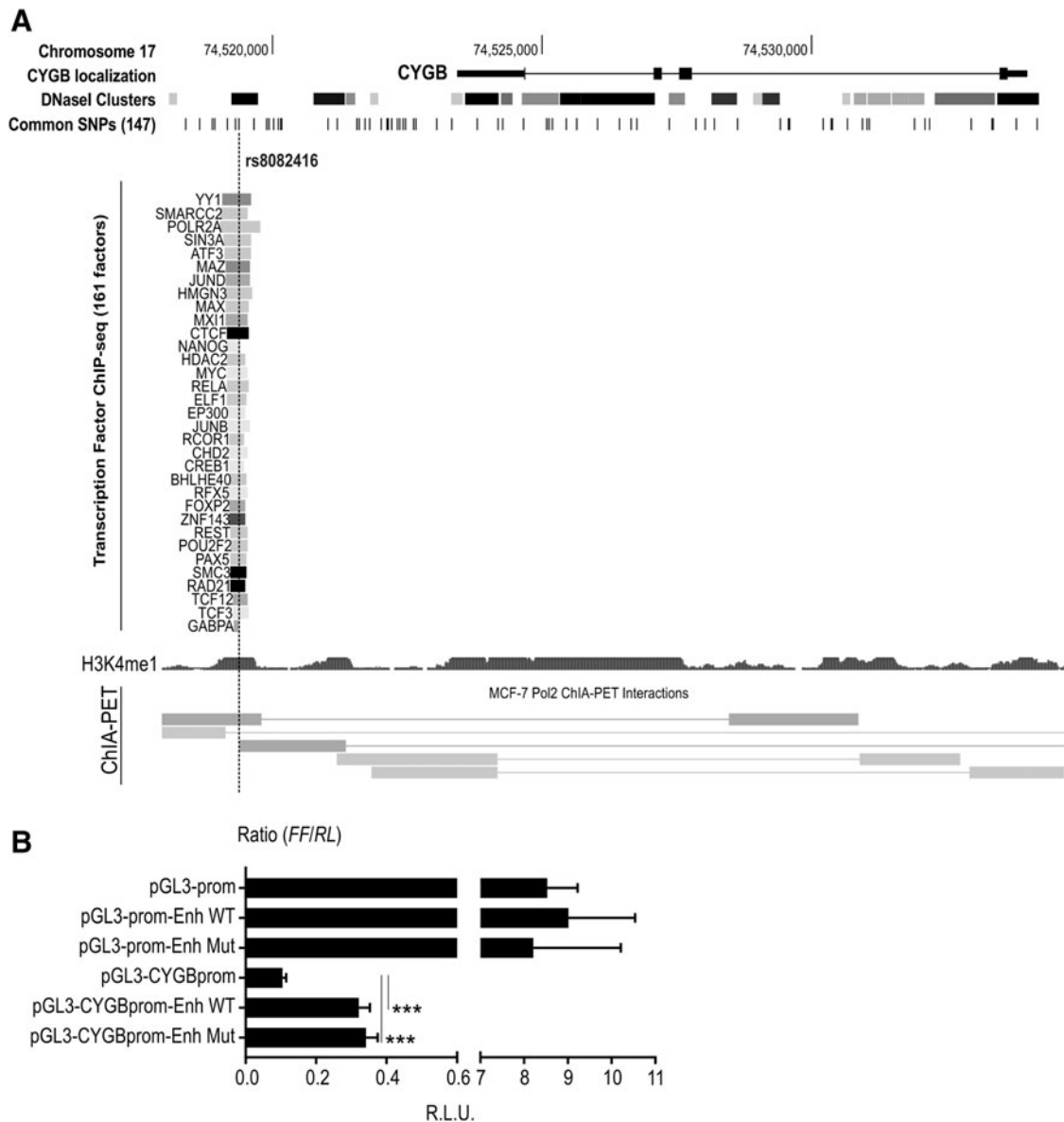
SUPPLEMENTARY FIG. S4. Transcript levels of the antioxidant genes *HO-1* and *HSP1A1* measured by RT-qPCR in WT, shCTR, shCYGB-1, and shCYGB-2 AB8/13 cells ($n = 4$). * $p < 0.05$; Student's *t*-test.



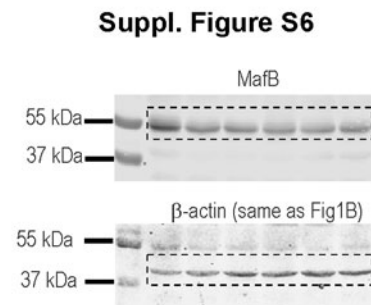
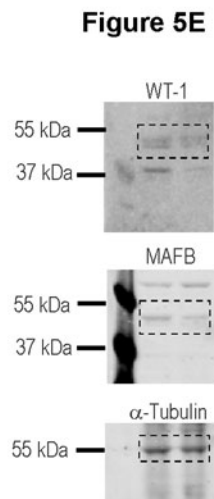
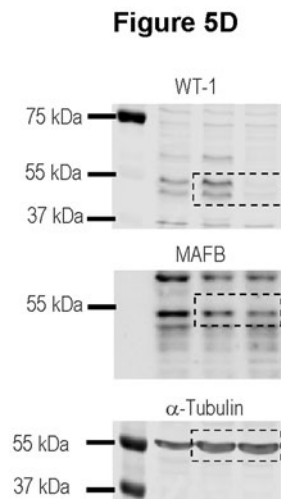
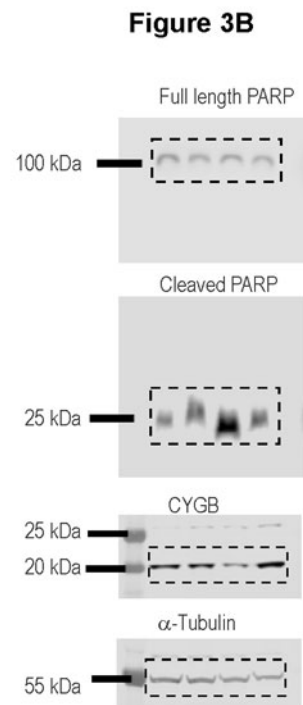
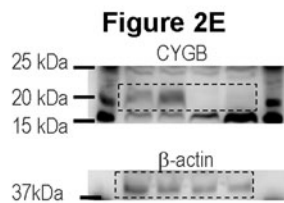
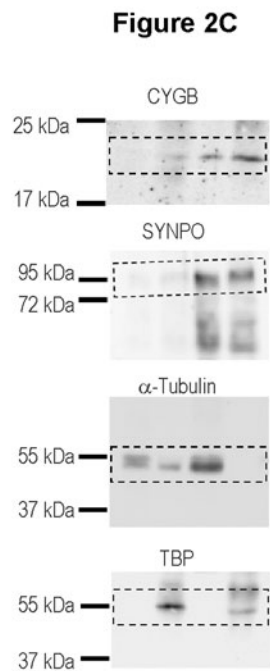
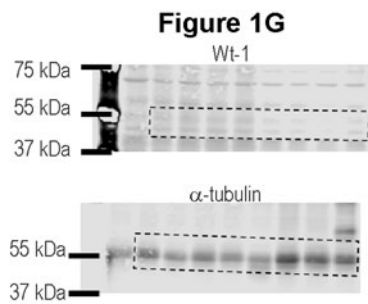
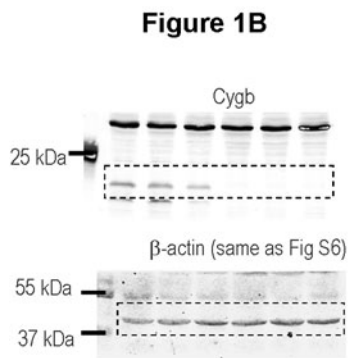
SUPPLEMENTARY FIG. S5. CYGB overexpression protects podocytes against ROS accumulation and cell death. (A) Efficacy of CYGB overexpression in AB8/13 cells ($n = 4$). ** $p < 0.01$; Student's *t* test. (B) Cell death measured by trypan blue exclusion. (C) Quantification of roGFP2 oxidation in nontreated (NT) and AMA-treated cells ($n = 4$). ** $p < 0.05$; ns, not significant; two-way ANOVA and Tukey correction for multiple comparisons. (D) Measurement of intracellular ROS accumulation by H_2DCFDA fluorescence ($n = 4$). *** $p < 0.001$; * $p < 0.05$; ns, not significant; two-way ANOVA and Tukey correction for multiple comparisons. (E) Corresponding cell death upon normal (NG) or high (HG) glucose treatment. Mannitol (NG + M) served as osmotic control. GUS (β -glucuronidase) overexpression was used as negative control for CYGB overexpression ($n = 4$). ** $p < 0.01$; ns, not significant; two-way ANOVA and Dunnett's correction for multiple comparisons. AMA, antimycin A; H_2DCFDA , 2',7'-dichlorodihydrofluorescein diacetate; ROS, reactive oxygen species.



SUPPLEMENTARY FIG. S6. Expanded RNA-sequencing data. (A) CYGB transcript levels in RPKM of multiple mapping in transcriptome analysis of WT and CYGB knockdown AB8/13 podocytes. (B) Mapping reads classification into total exons, introns, and intergenic regions. (C) Sample-to-sample distance and (D) principal component analysis of the RNA-sequencing data sets indicate clear separation among shCYGB and shCTR cells. RPKM, reads per kilobase per million mapped reads.



SUPPLEMENTARY FIG. S7. SNP rs8082416 coincides with a DNaseI hypersensitivity cluster and strong transcription factor occupancy. (A) University of California Santa Cruz Genome Browser output (*hg19*) of SNP rs8082416 and the *CYGB* gene locus illustrating that the SNP is located in the 3' intergenic region of *CYGB* and localized in a DNaseI hypersensitivity cluster with substantial transcription factor occupancy. *Gray saturation* is proportional to the maximum signal strength observed in any cell line. In addition, ChIA-PET interaction studies suggest loop formation between the SNP area and the first intron close to the transcription initiation region of the *CYGB* gene. (B) SV40 promoter (pGL3-prom)- and *CYGB* promoter (*CYGB*prom)-driven firefly luciferase reporter genes were transiently cotransfected into HEK293T cells. An enhancer fragment of 90 bp spanning the WT SNP rs8082416 (Enh WT) or mutated SNP (Enh Mut) was added to the SV40 promoter and *CYGB* promoter-driven firefly luciferase reporter genes. Results are displayed as ratios of firefly to *Renilla* luciferase activities in relative light units (R.L.U.) from three independent experiments performed in triplicate, error bars correspond to the standard error of mean. *** $p < 0.001$; Student's *t*-test. ChIA-PET, chromatin interaction analysis by paired-end tag; SNP, single-nucleotide polymorphism.



SUPPLEMENTARY FIG. S8. Original versions of immunoblots shown in Figures 1, 2, 3, 5, and S6.

Supplementary Table 1. Literature-based podocyte marker set. FC, Fold Change; FDR, False Discovery Rate; RPKM, Reads Per Kilobase Million mapped reads; SD, Standard Deviation

GENE	FC	FDR	shCTR_RPKM	shCTR_SD	shCYGB_RPKM	shCYGB_SD
ACTN4	1.09	1.00E+00	159.22	11.48	166.92	23.79
AKT2	-1.07	1.00E+00	7.23	0.2	6.45	0.73
ARHGDI A	1.27	2.70E-01	66.36	6.83	80.85	18.31
ATG5	1.19	2.37E-01	11.2	0.53	12.78	0.66
ATG7	-1.17	5.94E-01	4.85	0.2	3.96	0.53
ATP6AP2	1.2	7.48E-02	80.92	3.45	93.23	2.54
BRAF	1.17	4.53E-01	2.52	0.12	2.82	0.07
CD151	-1.14	5.44E-01	104.79	2.8	87.87	9.59
CD2AP	1.66	1.04E-09	20.69	1.19	32.95	2.08
CD2BP2	-1.07	1.00E+00	19.4	0.91	17.37	1.53
CD55	-1.27	5.79E-02	6.88	0.27	5.19	0.4
CDC42	1.18	2.50E-01	83.13	2.14	94.14	9.13
CEBPA	1.24	1.00E+00	0.11	0.02	0.13	0.03
CFL1	1.2	1.35E-01	172.92	11.17	198.25	16.25
CLIC5	1.92	1.00E+00	0	0.01	0.01	0.01
COL4A3	1.02	1.00E+00	0.03	0.02	0.03	0.01
CTSD	1.17	8.47E-01	93.03	11.25	104.49	19.63
DNM1	-1.12	1.00E+00	5.62	0.36	4.82	1.2
ENPEP	-1.97	9.49E-03	2.14	0.41	1.03	0.43
EXT1	1.3	4.86E-03	23.89	1.41	29.68	1.07
EZR	1.36	1.28E-04	109.15	7.08	142.4	4.14
FAT1	-1.08	1.00E+00	31.47	3.39	27.86	1.85
FLT1	-5.84	8.88E-03	0.05	0.02	0.01	0
FOXC1	1.02	1.00E+00	7.59	1.18	7.46	0.91
FOXC2	1.44	3.21E-02	3.26	0.58	4.48	0.43
FYN	1.25	4.38E-02	6.04	0.29	7.26	0.24
IGF1R	1.24	2.29E-01	6.87	1.22	8.18	0.19
INSR	1.04	1.00E+00	0.05	0.01	0.05	0.02
ITGB1	1.13	7.68E-01	446.48	13.27	481.68	48.65
KANK1	1.39	4.95E-04	2.72	0.14	3.64	0.11
KIRREL	-1.1	1.00E+00	52.01	2.8	45.27	5.09
KLF4	1.28	1.00E+00	0.67	0.22	0.82	0.07
KLF6	1.35	2.91E-04	22.27	0.89	28.86	0.86
LAMA5	-1.95	6.51E-03	4.96	0.98	2.45	1.11
LMX1B	-10.99	8.95E-01	0.02	0.02	0	0
MAFB	-86.2	1.78E-25	1.05	0.24	0.01	0.01
MAGI2	-1.58	7.90E-02	0.37	0.01	0.23	0.04
MDM2	-1.55	2.63E-09	81.88	3.62	50.51	2.02
MET	-1.25	4.30E-02	44.95	2.39	34.36	3.16
MPP5	1.39	3.85E-04	6.52	0.45	8.69	0.33
MTOR	1.07	1.00E+00	7.6	0.06	7.77	0.29

MYH9	1.32	1.53E-03	288.2	16.59	363.77	22.93
MYO1E	1.07	1.00E+00	21.87	1.43	22.33	0.88
NCK2	-1.34	2.28E-02	14.24	1	10.2	1.42
NDST1	1.42	2.46E-04	68.5	4.27	92.86	8.48
NPHS1	-2.85	1.00E+00	0.02	0.02	0.01	0.01
NPHS2	1	1.00E+00	0	0	0	0
NR2C2	1.03	1.00E+00	5.21	0.31	5.12	0.14
NRP1	-2.2	0.00E+00	32.87	0.26	14.29	2.22
OGT	1.27	2.03E-01	12.23	0.95	14.88	2.96
PDSS2	1.2	6.00E-01	2.81	0.06	3.23	0.37
PHB2	1.01	1.00E+00	43.5	0.94	42.14	0.27
PIK3C3	1.39	3.46E-04	3.58	0.19	4.76	0.13
PIK3R1	-1.34	3.56E-02	4.99	0.27	3.57	0.54
PIK3R2	1.43	1.02E-01	4.49	0.36	6.14	1.68
PLCE1	1.37	8.10E-03	2.29	0.22	2.99	0.23
PODXL	-3.68	1.74E-42	5.22	0.26	1.36	0.1
PPARG	3.65	5.10E-07	0.19	0.11	0.66	0.07
PRKCI	-1.05	1.00E+00	21.32	0.63	19.35	1.7
PTEN	-1.08	1.00E+00	7.75	0.4	6.87	0.11
PTPRO	-1.09	1.00E+00	0.05	0.01	0.05	0.02
RAC1	1.06	1.00E+00	96.66	2.33	97.68	3.94
RET	-6.72	2.48E-01	0.04	0.01	0	0.01
RHOA	1.06	1.00E+00	232.67	7.21	235.36	19.36
RHPN1	-1.21	1.00E+00	1.38	0.21	1.1	0.53
RICTOR	1.19	6.81E-01	3.6	0.22	4.09	0.69
ROBO2	1.6	1.00E+00	0	0	0.01	0.01
SCHIP1	-2.03	1.00E+00	0.21	0.12	0.1	0.14
SDC4	1.09	1.00E+00	433.89	32.22	455.05	89.71
SIRT1	-1.2	1.98E-01	7.84	0.24	6.26	0.18
SYNPO	-1.69	4.55E-04	2.91	0.55	1.65	0.25
TCF21	-1.69	2.24E-02	0.98	0.19	0.55	0.07
TJP1	1.13	6.65E-01	13.21	0.5	14.25	0.54
TLN1	1.24	2.24E-02	85.49	2.31	101.19	6.92
TSC1	1.37	1.68E-02	4.14	0.09	5.43	0.85
VANGL2	-1.19	3.11E-01	14.19	1.34	11.39	0.68
VEGFA	-1.46	8.62E-04	14.93	2.38	9.79	0.79
VHL	1.06	1.00E+00	11.83	0.64	12	1.11
WASL	1.14	6.38E-01	13.74	0.42	14.96	0.88
WT-1	-2.26	4.12E-02	0.97	0.13	0.41	0.35
XBP1	1.19	1.74E-01	23.22	0.55	26.37	0.52
YAP1	-1.23	3.31E-02	44.47	1.12	34.75	1.78

Supplementary Table 2. Single cell RNA-sequencing based podocyte marker set. FC, Fold Change; FDR, False Discovery Rate; RPKM, Reads Per Kilobase Million mapped reads; SD, Standard Deviation

GENE	FC	FDR	shCTR_RPKM	shCTR_SD	shCYGB_RPKM	shCYGB_SD
MT-ATP8	-1.05	1.00E+00	1365.92	119.72	1239.86	204.57
SDC4	1.09	1.00E+00	433.89	32.22	455.05	89.71
EZR	1.36	1.28E-04	109.15	7.08	142.40	4.14
CD59	1.24	5.99E-02	102.46	11.27	121.81	5.11
ARPC1A	-1.09	1.00E+00	68.31	6.55	60.28	3.47
HLA-A	1.41	1.11E-04	65.60	5.74	88.83	3.83
ALCAM	1.26	2.30E-02	48.37	1.89	58.48	5.10
ITGAV	1.79	8.44E-10	46.65	1.04	79.89	11.17
GPC1	-1.48	4.72E-02	46.33	4.12	30.13	9.74
GADD45A	-1.28	8.12E-03	44.29	0.55	33.05	1.07
ITGB5	-1.12	9.30E-01	35.92	1.87	30.82	2.05
CRYAB	1.37	3.69E-01	30.72	6.67	40.08	12.10
SEPT10	-1.01	1.00E+00	27.78	2.30	26.45	1.90
AIF1L	1.12	1.00E+00	25.14	0.53	27.00	3.26
RAB3B	1.65	2.04E-09	23.59	0.21	37.25	3.56
DPP4	-1.46	6.45E-03	22.70	1.37	14.93	3.56
NSF	1.43	4.25E-05	20.85	0.64	28.50	2.23
PARVA	1.32	1.62E-03	18.31	0.89	23.09	1.01
TMOD3	1.13	7.06E-01	17.49	1.23	18.92	0.77
GOLIM4	-1.24	7.62E-02	17.04	1.31	13.19	0.54
LGR4	-1.74	7.54E-10	16.98	1.16	9.35	1.02
AOX1	-1.17	1.00E+00	16.52	3.94	13.50	1.55
TSC22D1	-1.11	8.75E-01	16.41	0.34	14.18	0.51
FNBP1L	1.07	1.00E+00	16.12	1.49	16.44	2.17
VEGFA	-1.46	8.62E-04	14.93	2.38	9.79	0.79
ANXA4	1.06	1.00E+00	14.18	0.54	14.35	1.60
PAK1	1.11	8.95E-01	13.27	0.52	14.12	0.03
FGFR1	-1.30	1.61E-02	11.41	0.58	8.44	0.95
LPIN2	1.09	1.00E+00	10.94	0.27	11.47	0.45
CERS6	-1.04	1.00E+00	10.81	0.78	9.96	1.06
DNAJC11	1.15	5.46E-01	9.08	0.35	9.97	0.35
MOCS2	1.02	1.00E+00	8.18	1.03	7.97	1.34
ILDR2	1.16	7.26E-01	8.11	0.52	8.99	1.19
CTSV	-2.26	3.45E-14	7.83	0.64	3.33	0.54
MPP5	1.39	3.85E-04	6.52	0.45	8.69	0.33
ARHGEF18	1.45	4.60E-03	6.11	0.91	8.49	1.01
IFT80	-1.18	6.19E-01	5.78	0.50	4.70	0.51
PODXL	-3.68	1.74E-42	5.22	0.26	1.36	0.10
MTSS1	1.03	1.00E+00	4.91	0.71	4.85	0.45
CDKN1C	-2.47	3.74E-06	4.65	1.38	1.81	0.42
HAUS8	-1.27	1.73E-01	4.65	0.50	3.51	0.18

Supplementary Table 3. Altered pathways related to renal disease, based on Ingenuity Pathway Analysis. (B-H=Benjamini–Hochberg)

Category	B-H; p-value	Molecules
Glomerular Injury	4.66E-02; 6.2E-01	WT-1, CDKN1C, EDNF, ANLN, DCN, CDKN2C, SALL1, BUB1B, KCP, PDGFB, CTSV, BDKRB2, C4A/C4B, SCGB1A1, CAMK2A, CCL2, EDN1, WFDC2, RARB, LAMA1, ITGB4, SERPINE1, BDKRB1
Kidney Failure	2.44E-03; 3.89E-01	CACNA1S, GDNF, PDE4A, ACHE, C4A/C4B, AR, EDN1, TOP2A, CDH16, SERPINE1, GABRD, PDE11A, PPARG, GSTM1, WT-1, CACNA1D, GUCY1A3, FLT1, PDE4C, DCN, PTGS1, DRD2, BUB1B, KCP, G ABRE, NPPB, ITGAM, LDLR, NPR3, WFDC2, NPR1, SLC6A4, HMGR
Renal Necrosis / Cell Death	8.23E-02; 1E00	GAS7, MAP2K6, TCF4, SLC22A3, CTGF, PYCARD, TP73, IL32, EMP2, UNC5B, TMEFF2, PSEN2, NTN1, AR, EDN1, FGFR4, MCOLN3, MAP1LC3A, SLC22A2, RASSF5, PPARG, WT-1, APOBEC3B, NLRP3, FLT1, DCN, SALL1, LRRK2, IER3, ITPR1, IL24, BIRC5, CDK1, AREG, CCNB1, STRA6, PTH1R, IGFBP3, MAP3K8, MAFB, SFRP1, P2RX7, SLC47A1, RBP4
Nephrosis	1.74E-01; 1E00	CA2, SLC12A3, EMP2, PDE4A
Renal Degeneration	1.74E-01; 2.86E-01	CGB, CLDN16, HSD17B2
Renal Proliferation	1.74E-01; 4.28E-01	DLGAP5, GDNF, UNC5B, GDF9, TMEFF2, PLK1, CCDC8, AURKA, BIRC5, PDGFB, NTN1, FGFR3, PTGES, IGF2, EDN1, APLN, STEAP2, FGFR4, CDCA5, FBLN2, P2RX7, CEACAM1, OXTR
Renal Fibrosis	1.74E-01; 2.09E-01	BDKRB2, WT-1, CCL2, GDNF, WFDC2, DCN, BUB1B, BDKRB1, KCP
Renal Hydronephrosis	1.46E-01; 1.46E-01	SFRP2, MMP3, CCL2, DCN, NFIA, RARB, TGFB2, IMPA2, ITGB4, HSPA4L, TNFRSF11B
Renal Damage	9.8E-02; 5.95E-01	GSTM1, UNC5B, LRRK2, IGFBP5, CP, SLC38A3, NTN1, C4A/C4B, BDKRB2, PREX1, CAMK2A, EDN1, IGFBP3, HCK, TLR3, SLC22A2, ALOX5, SERPINE1, ITGB6, CRYM, C3AR1, BDKRB1, GJB2
Renal Atrophy	1.74E-01; 5.43E-01	DCN, SALL1, LRRK2, EFEMP1, BUB1B, HSPA4L
Renal Degradation	2.43E-01; 2.43E-01	LAMA1
Renal Inflammation	2.43E-01; 1E00	WT-1, SOCS1, TCF4, GDNF, DCN, IL21R, PTGS1, LRRK2, PSEN2, GPX7, C4A/C4B, SLC19A3, ITGAM, CCL2, TOP2A, TLR3, RASSF5, SERPINE1
Renal Nephritis	2.43E-01; 1E00	WT-1, SOCS1, TCF4, GDNF, DCN, IL21R, PTGS1, LRRK2, PSEN2, GPX7, C4A/C4B, SLC19A3, ITGAM, CCL2, TOP2A, TLR3, RASSF5, SERPINE1
Renal Cellular Infiltration	3.02E-01; 3.02E-01	LTB
Renal Hypoplasia	3.02E-01; 5.07E-01	RARB, PBX1, SALL1, PDGFB
Renal Dysfunction	3.11E-01; 3.11E-01	HPSE, VWF, ALOX5
Renal Tubule Injury	3.51E-01; 5.95E-01	GSTM1, EDN1, IGFBP3, IGFBP5, CP, SLC22A2, SERPINE1, CRYM, GJB2, SLC38A3
Renal Hypertrophy	4.14E-01; 6.2E-01	EDN1, GDNF, RARB, HSD17B2
Increased Levels of Albumin	4.19E-01; 4.19E-01	P2RX7
Renal Transformation	4.19E-01; 4.19E-01	WT-1
Renal Hyperplasia / Hyperproliferation	4.51E-01; 4.51E-01	WT-1, GDNF
Renal Dysplasia	6.68E-01; 6.68E-01	H19

Supplementary Table 4. Differentially expressed genes associated with oxidative stress and apoptosis in shCTGB vs shCTR.

Oxidative stress Gene ID	Fold change	FDR-corrected p-value	Apoptosis Gene ID	Fold change	FDR-corrected p-value
CAT	-1.58	7.28E-06	BCL2L11	-1.47	3.62E-04
CYGB	-28.92	1.10E-98	BID	1.52	2.74E-05
DHCR24	1.87	3.06E-12	BIRC3 (c-IAP1)	-1.57	8.81E-04
DUOX1	-18.36	2.20E-05	BIRC5	-3.83	1.25E-32
DUOX2	-12.61	3.09E-07	CASP1 (ICE)	-1.80	2.77E-04
FOXM1	-2.34	0.00E+00	CASP10 (MCH4)	-1.78	4.27E-07
GCLC	1.51	5.14E-05	CASP3	1.51	2.84E-05
GPX3	-4.69	9.97E-19	CD40 (TNFRSF5)	-1.52	1.00E-02
GPX7	-2.89	1.00E-02	DAPK1	1.62	2.27E-08
NCF2	3.29	3.63E-37	FAS (TNFRSF6)	-1.53	1.21E-06
NUDT1	-1.62	5.04E-06	PYCARD (TMS1/ASC)	-2.73	2.72E-06
PRDX2	-1.81	3.82E-14	TNFRSF11B	-2.02	0.00E+00
PREX1	-4.71	8.03E-08	TNFRSF9	3.03	2.31E-24
PTGS1 (COX1)	-2.44	3.33E-04	TP73	-2.45	2.05E-08
PTGS2 (COX2)	-1.66	3.00E-02			
SOD3	-3.70	8.01E-04			
UCP2	-1.91	1.14E-09			

Supplementary Table 5. Primers used for RT-qPCR quantification

mRNA	Forward primer (5'-3')	Reverse primer (5'-3')	Amplico size (bp)
<i>CYGB</i>	CAAGGTGGAACCGGTGTACT	TCACGTGGCTGTAGATGAGG	137
<i>DUOX1</i>	CAGCTGGAAGAGGAAAACAAGG	TGCAGAGTGTGTTCCCTTAGGC	138
<i>DUOX2</i>	GAAGGCTGTGACAAAGCAGC	AACATGTCCTGGGGCTTGAG	201
<i>GPX3</i>	AACTCCTGTCCTCCCACCTC	ATCTTGACGTTGCTGACCGT	167
<i>GPX7</i>	GCAGGAGCAGGACTTCTACG	CTCGGTAGTGCTGGTCTGTG	137
<i>HO-1</i>	ATGACACCAAGGACCAGAGC	GTGTAAGGACCCATCGGAGA	153
<i>HSP1A1</i>	TGCTGATCCAGGTGTACGAG	CGTTGGTGATGGTGATCTTG	204
<i>L28</i>	GCAATTCCTTCCGCTACAAC	TGTTCTTGCGGATCATGTGT	198
<i>MAFB</i>	TCGACCTGCTCAAGTTCGAC	AGTTGCTCGCCATCCAGTAC	204
<i>PYCARD</i>	GCCGAGGAGCTCAAGAAGTT	ATAAAGTGCAGGCCTGGCTT	296
<i>SERPINE1</i>	GACCTCAGGAAGCCCCTAGA	ACTGTTCCCTGTGGGGTTGTG	275
<i>SOD3</i>	CGAGACATGTACGCCAAGGT	AACTGGTGACGCTGGATGG	248
<i>TP73</i>	CGAAAATGCCAACAAACGGC	AGATTGAACTGGGCCGTGG	247
<i>WT-1</i>	GCGGAGCCCAATACAGAATA	TCTCACCAGTGTGCTTCCTG	207
<i>Cygb</i>	CCATCCTGGTGAGGTTCTTTGT	GATCCTCCATGTGTCTAAACTG	75
<i>Wt-1</i>	GCCTTCACCTTGCACTTCTC	GACCGTGCTGTATCCTTGGT	186
<i>Mafb</i>	TGGTGTTCAAGTCCCTTCCG	TCCTCTTACTGACCCGCAGA	95
<i>s12</i>	GAAGCTGCCAAAGCCTTAGA	AACTGCAACCAACCACCTTC	214
<i>Atp6v1g2</i>	AGTGAAAACGGGAGCGCTAA	GCCTTCCTCTTCCCTGGCATC	222
<i>Cox7c</i>	AGGGTCCGGGGAAGAATTTG	AAAGAAAGGTGCGGCAAACC	101
<i>Atp6v0a4</i>	AGGCTGCGTATTGCTGTGTA	TAGAGTCGTCTCCAGGGTGAT	242
<i>Ucp2</i>	GCGGTCCGGACACAATAGTA	GGGACCTTCAATCGGCAAGA	216
<i>Ndufab1</i>	TGGAAGACGAATTTGGGTTTGAA	TGGCAATGACAAGAGAAGTGGA	140
<i>Angpt2</i>	GCACAAAGGATTCCGACAAT	AAGTTGGAAGGACCACATGC	94
<i>Fit1</i>	TGAGGAGCTTTCACCGAACT	TATCTTCATGGAGGCCTTGG	130
<i>Tgf-b1</i>	GAGCCCGAAGCGGACTACT	TTGCGGTCCACCATTAGCA	59
<i>Acta2</i>	TCCCTGGAGAAGAGCTACGAACT	AAGCGTTCGTTTCCAATGGT	62
<i>Vegfa</i>	CAGGCTGCTGTAACGATGAA	GCATTCACATCTGCTGTGCT	140
<i>Pecam1 (Cd31)</i>	AACAGAAACCCGTGGAGATG	GGCTTCCACACTAGGCTCAG	86
<i>Plau</i>	CCTACAATGCCACAGACCT	CAAACCTGCCTTAGGCCAATC	120

Supplementary Table 6. Details of RNA-sequencing mapping statistics.

Sample	# of raw reads	# of pre-processed reads	% pre-processed reads	# of mapped reads	% mapped reads	% reads mapped to exon region	% reads mapped to intronic region	% reads mapped to intergenic region
shCTR-A	30,153,616	26,976,062	89.46	25,777,431	95.56	89.8	8.9	1.3
shCTR-B	29,171,024	26,084,110	89.42	24,885,595	95.41	89.41	9.22	1.37
shCTR-C	28,754,530	25,656,745	89.23	24,522,454	95.58	90.53	8.19	1.28
shCYGB-A	27,097,202	24,260,728	89.53	23,267,165	95.90	90.8	8.02	1.18
shCYGB-B	28,167,338	25,193,444	89.44	24,351,185	96.66	90.08	8.75	1.16
shCYGB-C	26,183,974	23,419,816	89.44	22,439,161	95.81	88.91	9.85	1.24